Electronic Supplementary Material (ESI) for Chemical Communications.

Chirality sensing of choline derivatives by a triple anion helicate cage through induced circular dichroism

Wei Zuo, Zhe Huang, Yanxia Zhao, Wenhua Xu, Zhihua Liu, Xiao-Juan Yang, Chuandong Jia,* and Biao Wu*

Key Laboratory of Synthetic and Natural Functional Molecule Chemistry of the Ministry of Education, College of Chemistry and Materials Science, Northwest University, Xi'an 710127, China

Table of Contents

1. General considerations

2. Synthesis of chiral guest compounds

3. NMR spectra of host-guest complexes

4. Crystal structural data of $(TBA)_5[(\pm\mathbf{G1})\subset(PO_4)_2\mathbf{L}_3]$

5. NMR and HRMS studies of $(\pm)\mathbf{G1}\subset\mathbf{H}$

6. Density Functional Theory (DFT) computations

7. CD spectra of guests and host-guest complexes

8. CD titrations

1. General considerations

All reagents were obtained commercially and used without further purification. All NMR spectra were obtained at 20 ^{o}C by using a Bruker AVANCE III-400 MHz spectrometer. ESI-MS measurements were carried out using a Bruker micrOTOF-Q II ESI-Q-TOF LC/MS/MS spectrometer. Melting points were detected on an X-4 Digital Vision MP instrument. The Circular dichroism (CD) spectra were recorded on a J-1500 spectropolarimeter (Jasco, Japan), using a 1 cm quartz cuvette.

X-ray diffraction data were collected on a Bruker SMART APEX II diffractometer at 123 K with graphite-monochromated Mo Kα radiation (λ = 0.71073 Å). An empirical absorption correction using SADABS was applied for the data. The structures were solved by direct methods using the SHELXS-2014 program. All non-hydrogen atoms were refined anisotropically by full-matrix least-squares on F^2 by the use of the program SHELXL-2014, and hydrogen atoms were included in idealized positions with thermal parameters equivalent to 1.2 times those of the atom to which they were attached. In the Checkcif file, alerts at level B were reported in the crystal of (±)**G1⊂H**. The alerts were induced by non-reasonable atom distances in one tetrabutylammonium counter cation, which was found to be severely disordered though low temperature 123 K was used for the data collection. Another alert was induced by a severely disordered Et_2O molecule with 172 electrons per unit cell, which was removed from the unit cell by the SQUEEZE command. The removed 172 electrons could correspond with the removal of 2.0 molecules of Et_2O per formula unit.

2. Synthesis of chiral guest compounds

(*R*)-**G3** and (*S*)-**G3** are commercially available and were used as received. (*R*)-**G6** and (*S*)-**G6** are known compounds.[1] Other guests were synthesized with a general method as described in the following:

2.1 Synthesis of the iodide salts

The iodide salts of other guests were synthesized by reaction of a corresponding amine (4.0 mmol) with MeI (1.25 mL, 20 mmol) and K_2CO_3 (2.76 g, 20 mmol) in MeCN (15 mL). After overnight reaction at room temperature, the suspended solid was removed by filtration and the solution was dried over vacuum to yield the iodide salts as white powders.

2.2 Synthesis of the hexafluorophosphate salts

An aqueous solution of the iodide salt of **G1** or **G2** was mixed with an aqueous solution of KPF_6 (equal molar amount) and stirred extensively for 1 h under room temperature. The solution was then dried over vacuum and MeCN was added to the solid thus obtained. After extensive stirring for 1 h, the suspended solid was filtrated off and the clear solution was dried over vacuum to yield the corresponding hexafluorophosphate salt. The iodide salts of **G4**−**G7** were converted to hexafluorophosphate salts according to a previously reported literature.[1]

(R)-**G1:** white solid obtained in a total yield of 65 %.^{1}H NMR (400 MHz, MeCN-d_3, ppm): δ 3.95 (m, 1H), 3.74 (m, 1H), 3.63 (t, J = 5.2 Hz, 1H) 3.46 (m, 1H), 3.06 (s, 9H), 1.37 (dt, J = 6.8 Hz, J = 2.0 Hz, 3H), ^{13}C NMR (100 MHz, MeCN-d_3): δ 72.1, 61.2, 53.0, 12.3. HRMS (ESI): *m/z* calcd for $[M\text{-}PF_6]^+$ $C_6H_{16}NO^+$: 118.1226; found: 118.1223.

(S)-**G1:** white solid obtained in a total yield of 61%. ^{1}H NMR (400 MHz, MeCN-d_3, ppm): δ 3.95 (m, 1H), 3.74 (m, 1H), 3.63 (t, J = 5.2 Hz, 1H) 3.46 (m, 1H), 3.06 (s, 9H), 1.37 (dt, J = 6.8 Hz, J = 2.0 Hz, 3H), ^{13}C NMR (100 MHz, MeCN-d_3): δ 72.1, 61.2, 53.0, 12.3. HRMS (ESI): *m/z* calcd for $[M\text{-}PF_6]^+$ $C_6H_{16}NO^+$: 118.1226; found: 118.1223.

(R)-**G2:** white solid obtained in a total yield of 64%. ^{1}H NMR (400 MHz, MeCN-d_3, ppm): δ 4.35 (m, 1H), 3.72 (d, J = 8 Hz, 1H), 3.28 (m, 2H), 3.15 (s, 9H), 1.19 (d, J = 8 Hz, 3H). ^{13}C NMR (100 MHz, MeCN-d_3): δ 72.0, 62.6, 55.2, 22.1. HRMS (ESI): *m/z* calcd for $[M\text{-}PF_6]^+$ $C_6H_{16}NO^+$: 118.1226; found: 118.1223.

(S)-**G2:** white solid obtained in a total yield of 62%. ^{1}H NMR (400 MHz, MeCN-d_3, ppm): δ 4.35 (m, 1H), 3.72 (d, J = 8 Hz, 1H), 3.28 (m, 2H), 3.15 (s, 9H), 1.19 (d, J = 8 Hz, 3H). ^{13}C NMR (100 MHz, MeCN-d_3): δ 72.0, 62.6, 55.2, 22.1. HRMS (ESI): *m/z* calcd for $[M\text{-}PF_6]^+$ $C_6H_{16}NO^+$: 118.1226; found: 118.1223.

(R)-**G4**: white solid obtained in a total yield of 73%. M.p.: 155-156 ℃. ^{1}H NMR (400 MHz, MeCN-d_3, ppm): δ 7.55-7.50 (m, 5H), 4.56 (q, J = 8 Hz, 1H), 2.94 (s, 9H), 1.75 (dt, J = 6.8 Hz, J = 2.0 Hz, 3H). ^{13}C NMR (100 MHz, MeCN-d_3): δ 133.9, 131.6, 131.5, 130.1, 75.2, 52.0, 15.4. HRMS (ESI): *m/z* calcd for $[M\text{-}PF_6]^+$ $C_{11}H_{18}N^+$: 164.1434; found: 164.1431.

(S)-**G4**: white solid obtained in a total yield of 71%. M.p.: 155-156 ℃. ^{1}H NMR (400 MHz, MeCN-d_3, ppm): δ 7.55-7.50 (m, 5H), 4.56 (q, J = 8 Hz, 1H), 2.94 (s, 9H), 1.75 (dt, J = 6.8 Hz, J = 2.0 Hz , 3H). ^{13}C NMR (100 MHz, MeCN-d_3): δ 133.9, 131.6, 131.5, 130.1, 75.2, 52.0, 15.4. HRMS (ESI): *m/z* calcd for $[M\text{-}PF_6]^+$ $C_{11}H_{18}N^+$: 164.1434; found: 164.1431.

(R)-**G5**: white solid obtained in a total yield of 72%. M.p.: 156-157 ℃. ^{1}H NMR (400 MHz, MeCN-d_3, ppm): δ 7.43 (d, J = 8.0 Hz, 2H), 7.03 (d J = 9.2 Hz, 2H), 4.50 (q, J = 8.0 Hz, 1H), 3.83 (s, 3H), 2.91 (s, 9H), 1.72 (dt, J = 7.2 Hz, J = 2 Hz, 3H). ^{13}C NMR (100 MHz, MeCN-d_3): δ 162.2, 132.9, 125.7, 115.3, 74.9, 56.2, 51.7, 15.4. HRMS (ESI): *m/z* calcd for $[M\text{-}PF_6]^+$ $C_{12}H_{20}NO^+$: 194.1539; found: 194.1536.

(S)-**G5**: white solid obtained in a total yield of 76%. M.p.: 156-157 ℃. ^{1}H NMR (400 MHz, MeCN-d_3, ppm): δ 7.43 (d, J = 8.0 Hz, 2H), 7.03 (d J = 9.2 Hz, 2H), 4.50 (q, J = 8.0 Hz, 1H), 3.83 (s, 3H), 2.91 (s, 9H), 1.72 (dt, J = 7.2 Hz, J = 2Hz, 3H). ^{13}C NMR (100 MHz, MeCN-d_3): δ 162.2, 132.9, 125.7, 115.3, 74.9, 56.2, 51.7, 15.4. HRMS (ESI): *m/z* calcd for $[M\text{-}PF_6]^+$ $C_{12}H_{20}NO^+$: 194.1539; found: 194.1536.

(R)-**G7**: white solid obtained in a total yield of 68%. M.p.: 159-160 ℃. ^{1}H NMR (400 MHz, MeCN-d_3, ppm): δ 3.18 (q, J = 8.0 Hz, 1H), 2.96 (s, 9H), 1.98 (m, 1H). 1.79-1.56 (m, 5H), 1.48-1.33 (m, 2H), 1.29 (dt, J = 8.0 Hz, J = 2.0 Hz , 3H), 1.25-1.10 (m, 3H). ^{13}C NMR (100 MHz, MeCN-d_3): δ 77.3, 52.2, 37.8, 33.7,

28.7, 27.4, 26.6, 26.4, 10.5. HRMS (ESI): *m/z* calcd for $[M\text{-}PF_6]^+$ $C_{11}H_{24}N^+$: 170.1903; found: 170.1901.

(S)-**G7**: white solid obtained in a total yield of 70%. M.p.: 159-160 ℃. ^{1}H NMR (400 MHz, MeCN-d_3, ppm): δ 3.18 (q, J = 8.0 Hz, 1H), 2.96 (s, 9H), 1.98 (m, 1H). 1.79-1.56 (m, 5H), 1.48-1.33 (m, 2H), 1.29 (dt, J = 8.0 Hz, J = 2.0 Hz, 3H), 1.25-1.10 (m, 3H). ^{13}C NMR (100 MHz, MeCN-d_3): δ 77.3, 52.2, 37.8, 33.7, 28.7, 27.4, 26.6, 26.4, 10.5. HRMS (ESI): *m/z* calcd for $[M\text{-}PF_6]^+$ $C_{11}H_{24}N^+$: 170.1903; found: 170.1901.

2.3. ^{1}H NMR and ^{13}C NMR spectra of the new compounds.

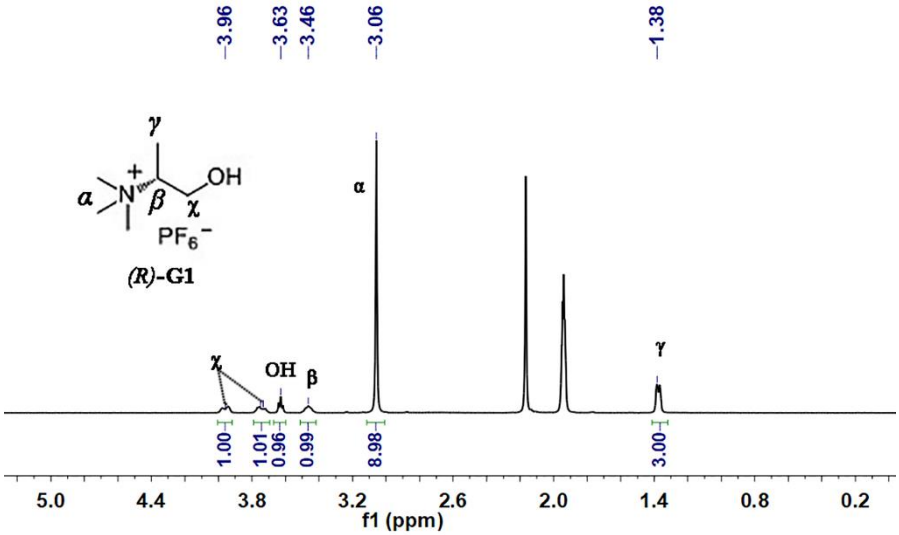

Fig. S1. ^{1}H NMR spectrum (400 MHz, MeCN-d_3) of *(R)*-**G1**.

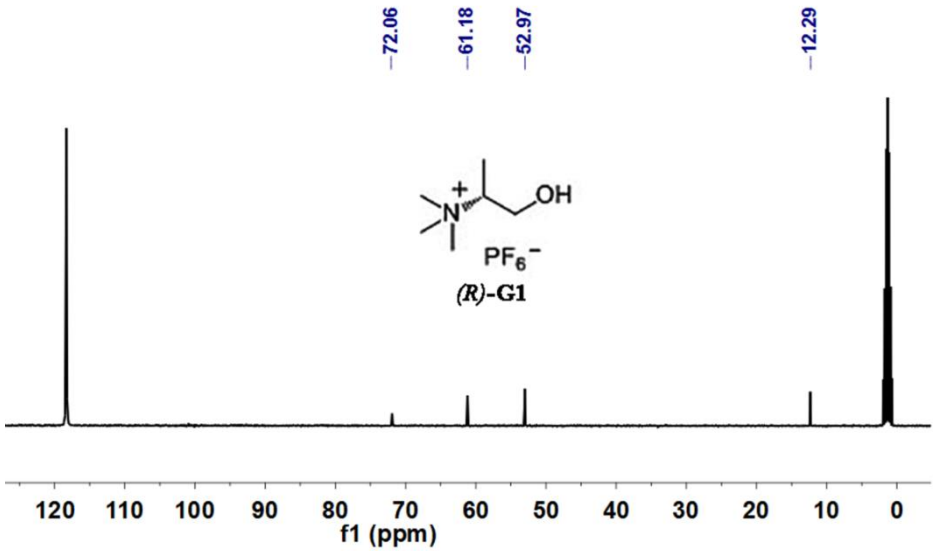

Fig. S2. ^{13}C NMR spectrum (100 MHz, MeCN-d_3) of *(R)*-**G1**.

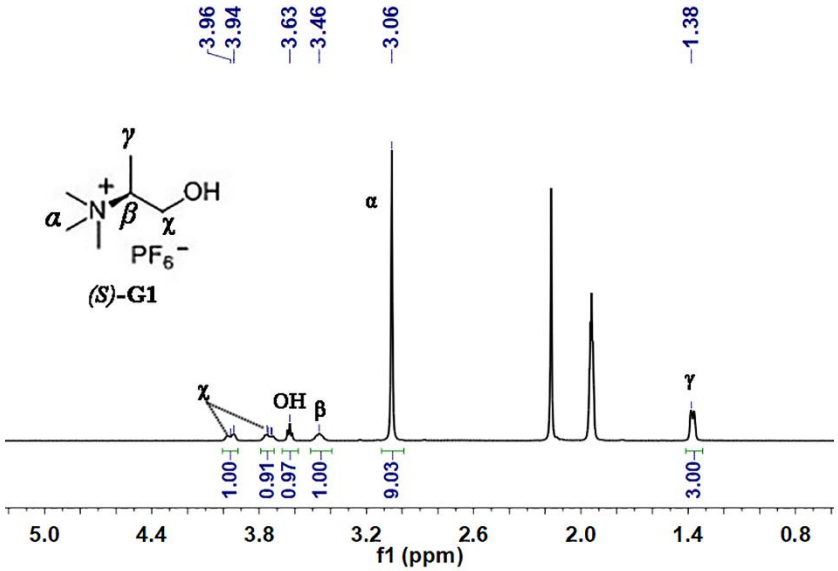

Fig. S3. ^{1}H NMR spectrum (400 MHz, MeCN-d_3) of *(S)*-**G1**.

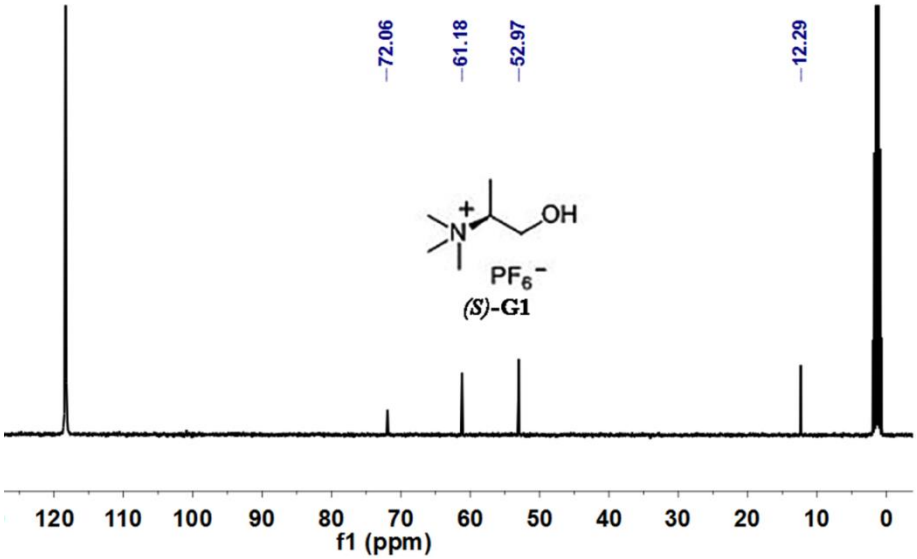

Fig. S4. ^{13}C NMR spectrum (100 MHz, MeCN-d_3) of *(S)*-**G1**.

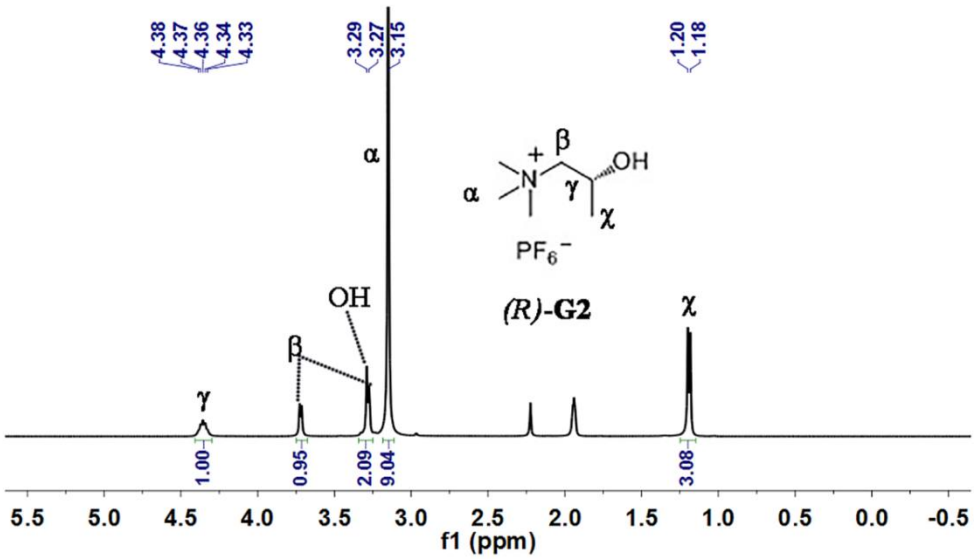

Fig. S5. ^{1}H NMR spectrum (400 MHz, MeCN-d_3) of *(R)*-**G2**.

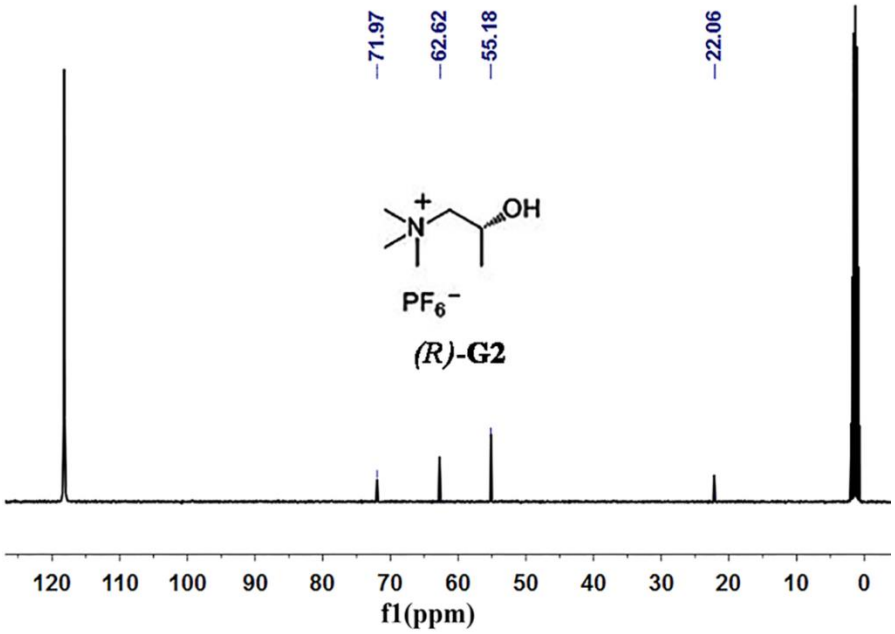

Fig. S6. ^{13}C NMR spectrum (100 MHz, MeCN-d_3) of *(R)*-**G2**.

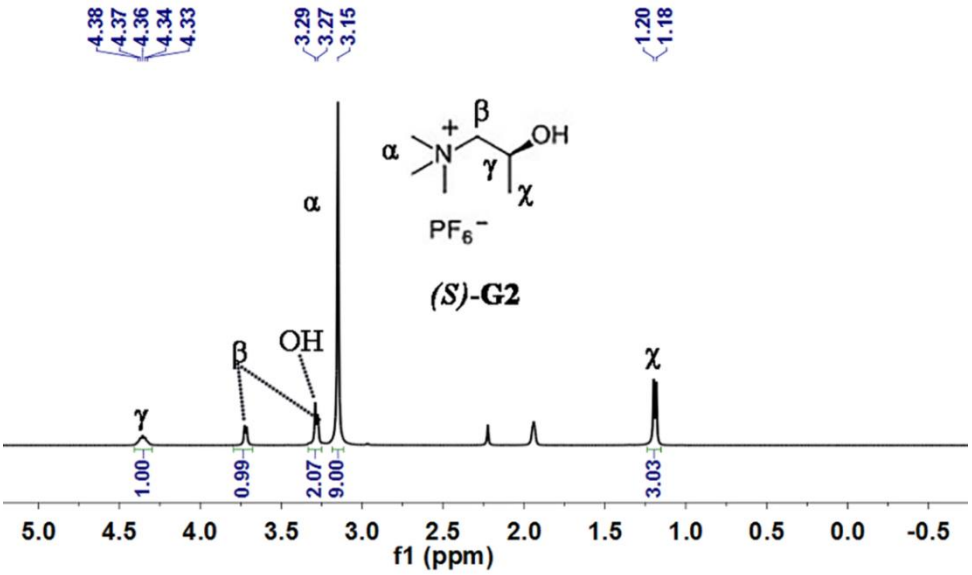

Fig. S7. ^{1}H NMR spectrum (400 MHz, MeCN-d_3) of *(S)*-**G2**.

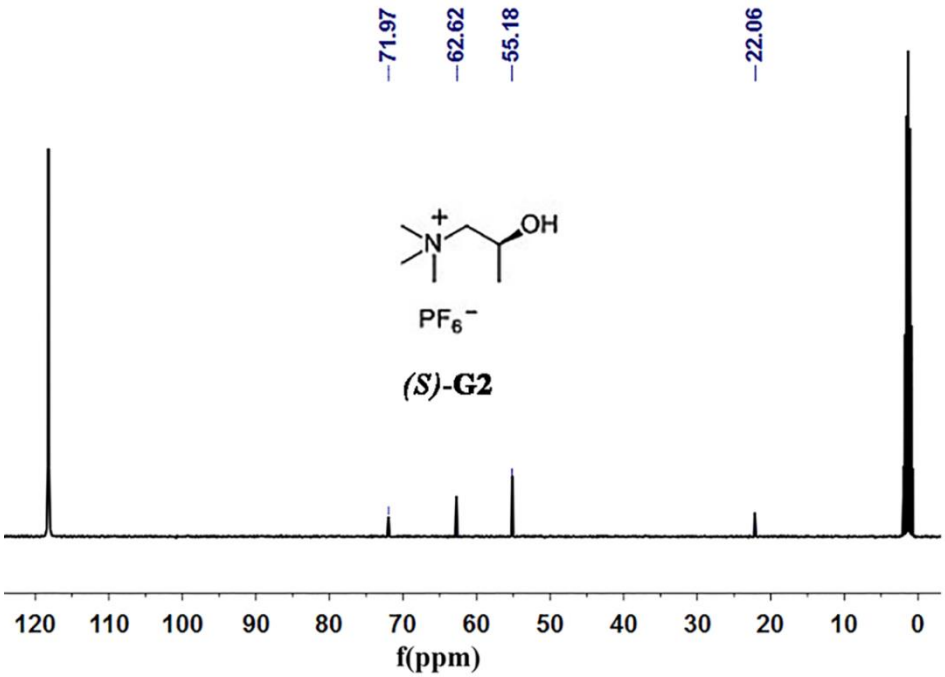

Fig. S8. ^{13}C NMR spectrum (100 MHz, MeCN-d_3) of *(S)*-**G2**.

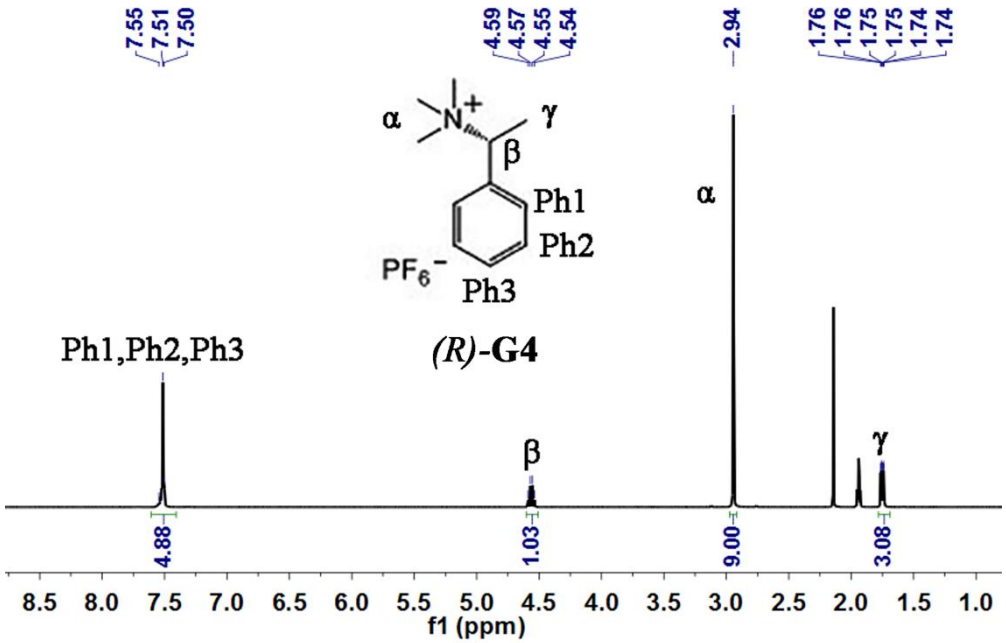

Fig. S9. ^{1}H NMR spectrum (400 MHz, MeCN-d_3) of *(R)*-**G4**.

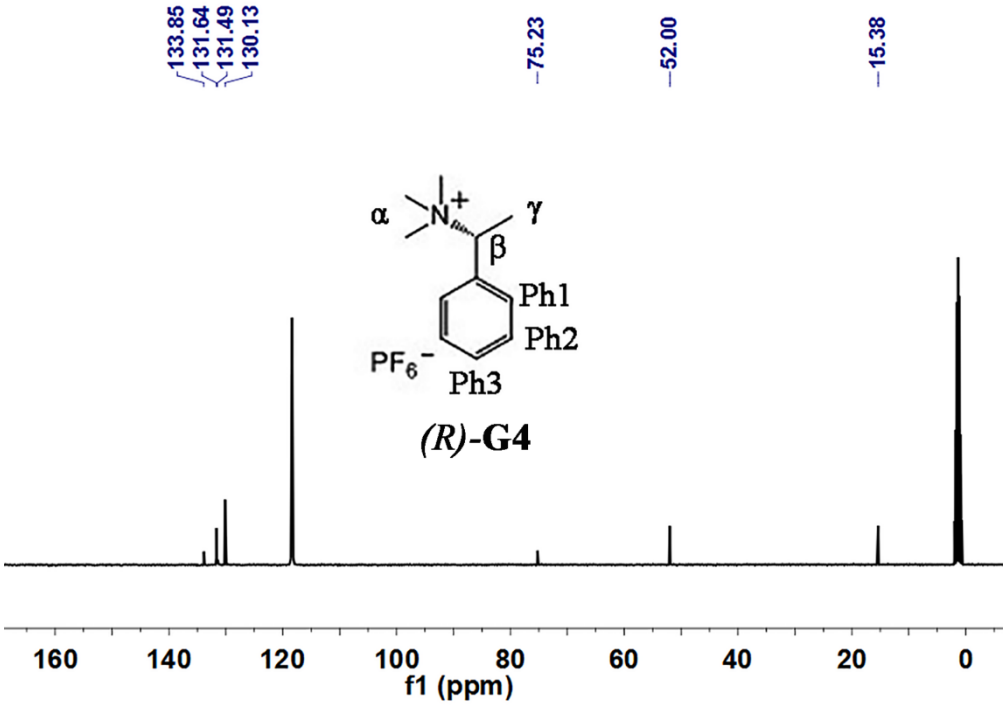

Fig. S10. ^{13}C NMR spectrum (100 MHz, MeCN-d_3) of *(R)*-**G4**.

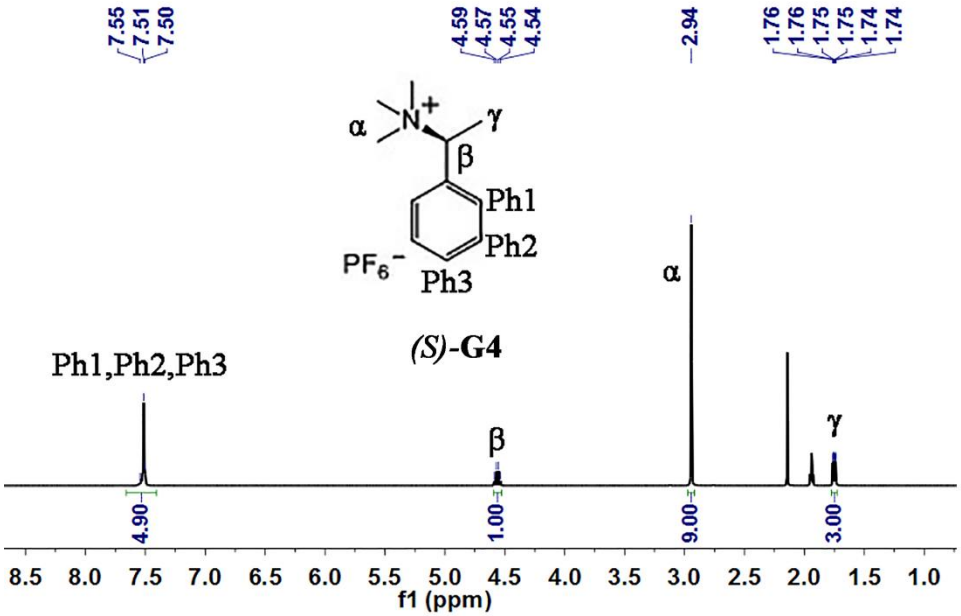

Fig. S11. ^{1}H NMR spectrum (400 MHz, MeCN-d_3) of *(S)*-**G4**.

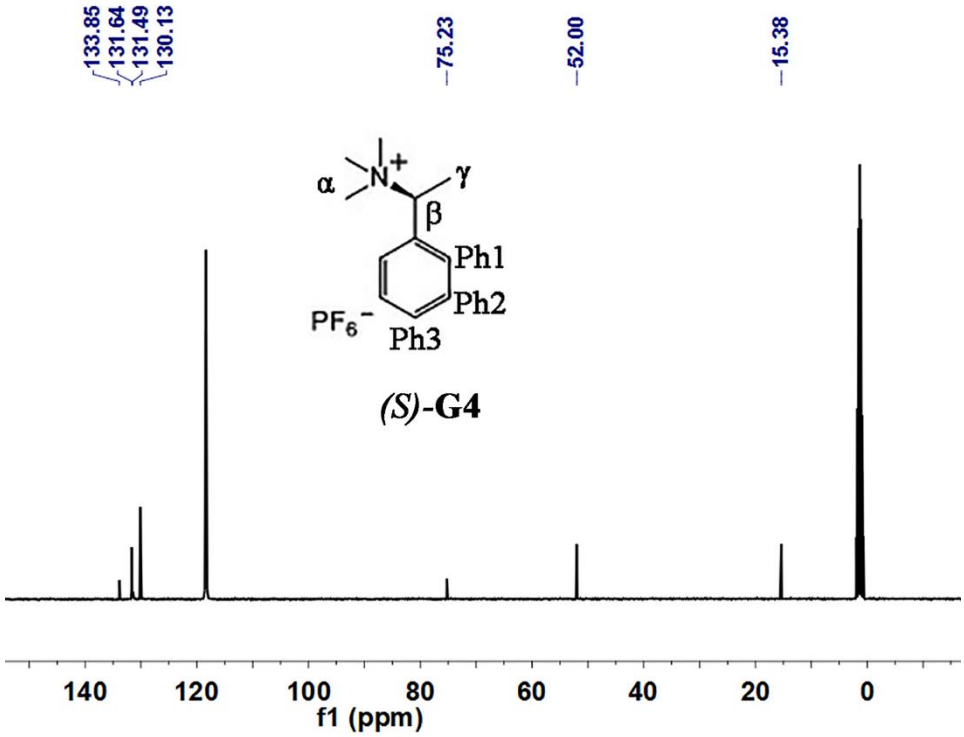

Fig. S12. ^{13}C NMR spectrum (100 MHz, MeCN-d_3) of *(S)*-**G4**.

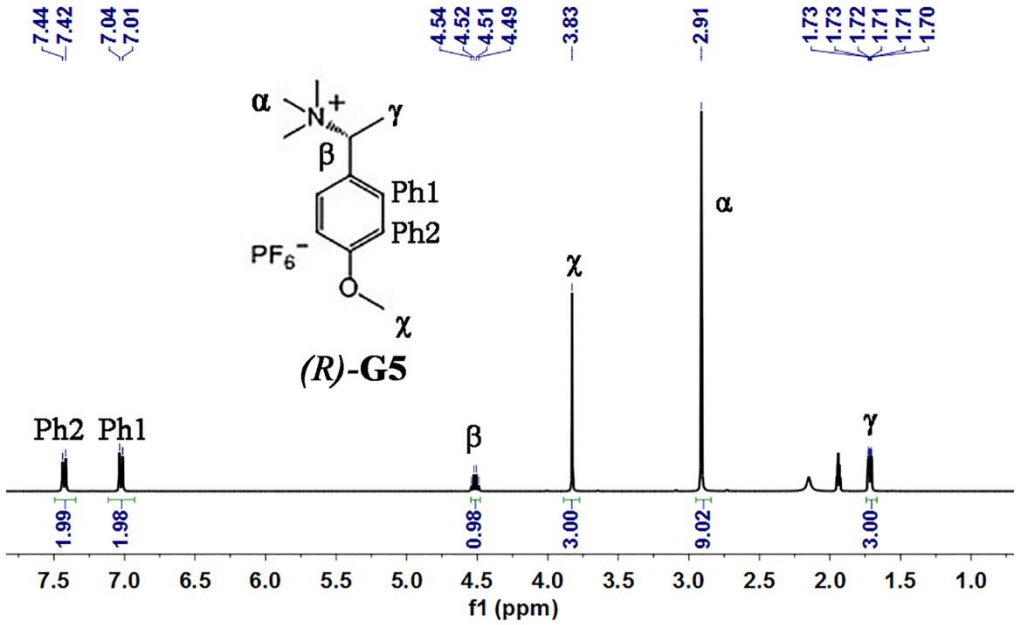

Fig. S13. ^{1}H NMR spectrum (400 MHz, MeCN-d_3) of *(R)*-**G5**.

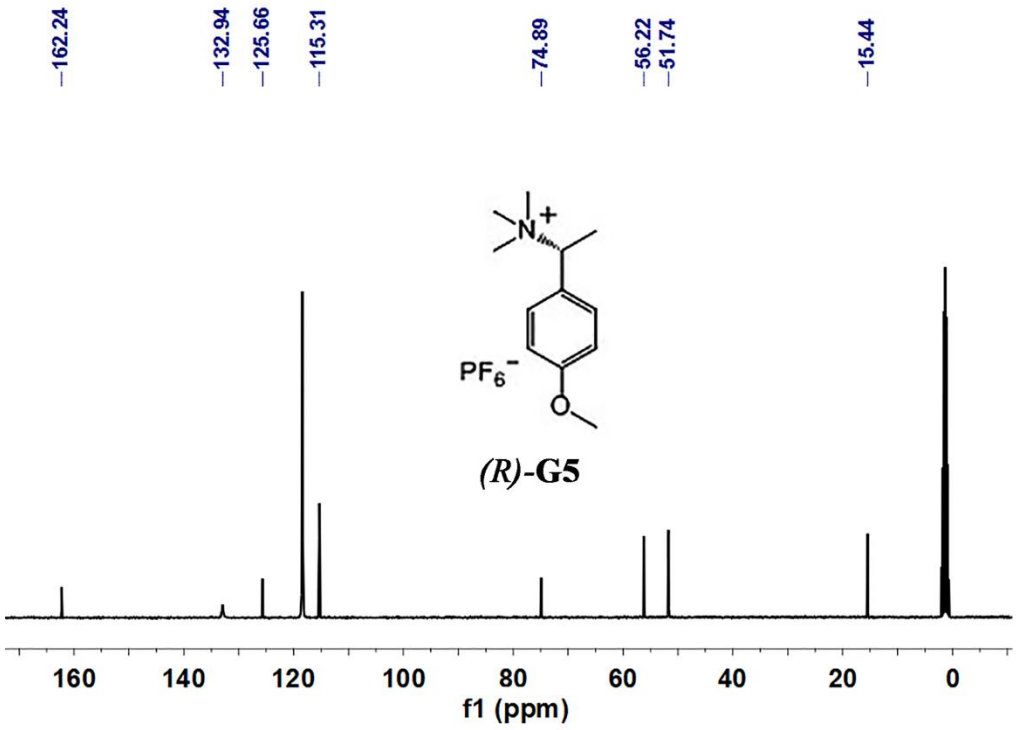

Fig. S14. ^{13}C NMR spectrum (100 MHz, MeCN-d_3) of *(R)*-**G5**.

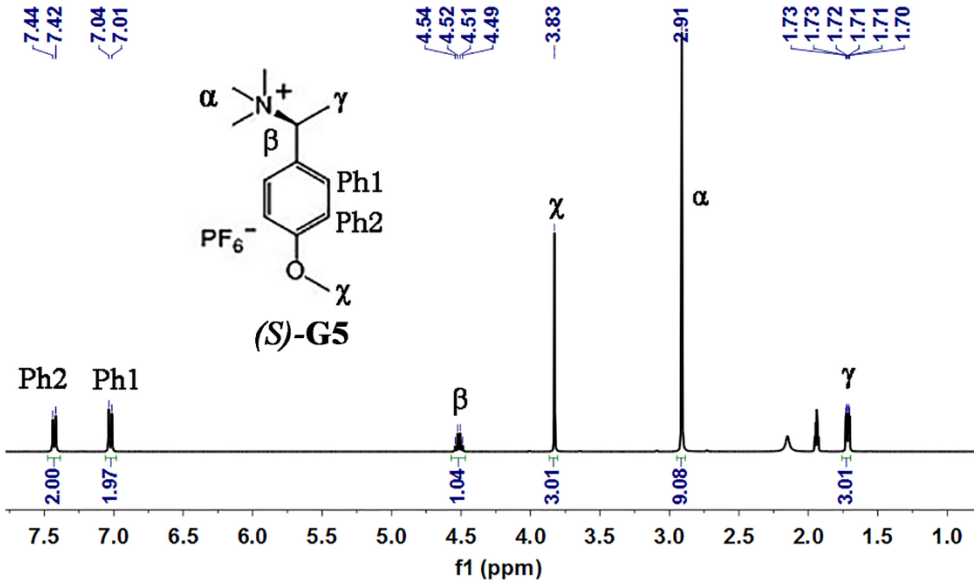

Fig. S15. ^{1}H NMR spectrum (400 MHz, MeCN-d_3) of *(S)*-**G5**.

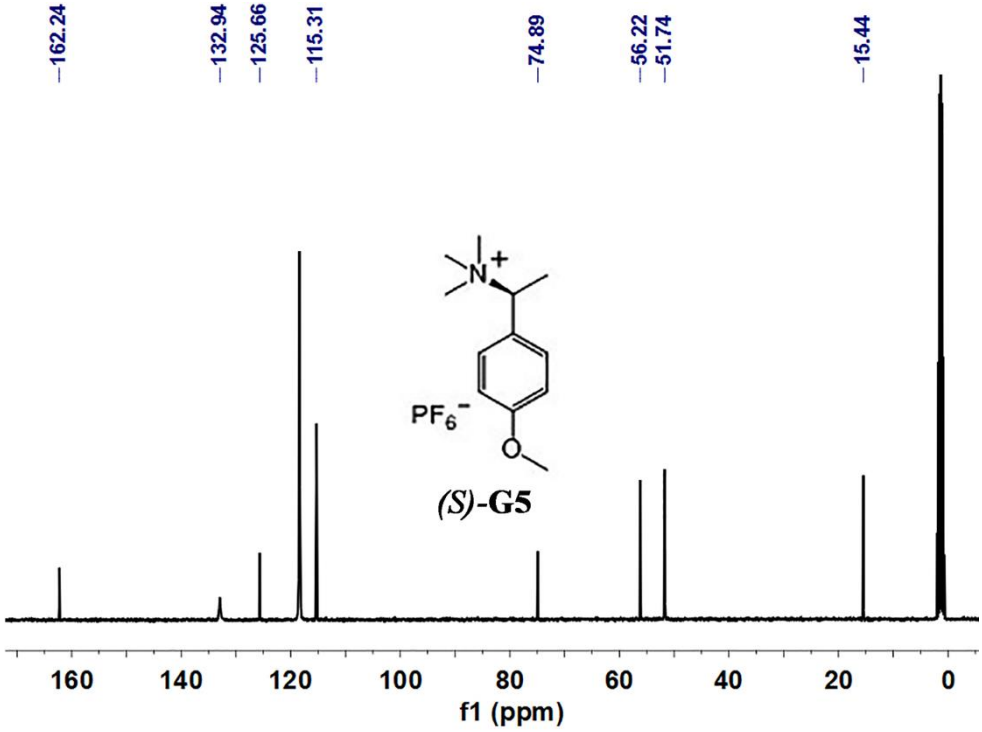

Fig. S16. ^{13}C NMR spectrum (100 MHz, MeCN-d_3) of *(S)*-**G5**.

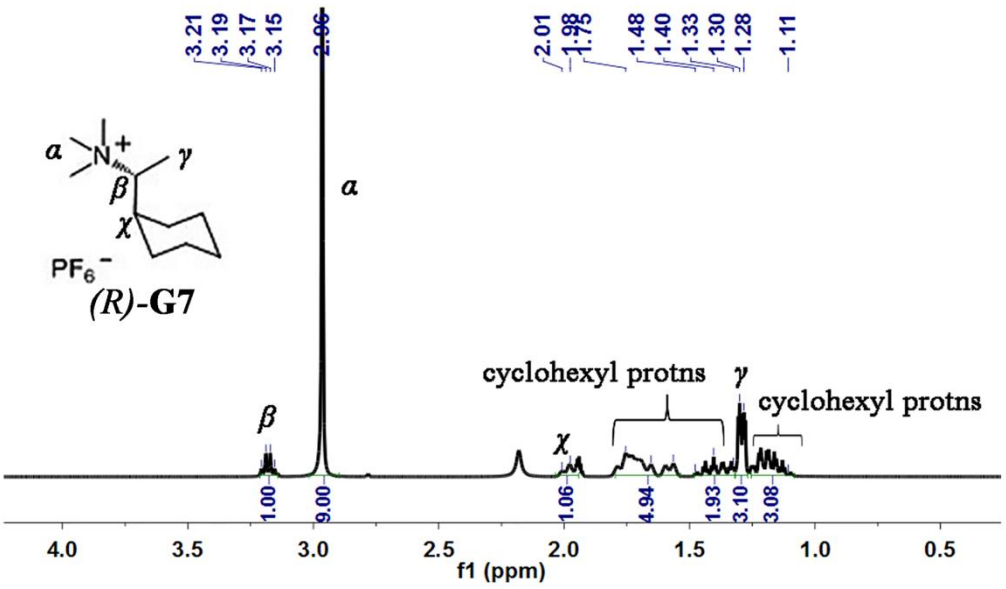

Fig. S17. ^{1}H NMR spectrum (400 MHz, MeCN-d_3) of *(R)*-**G7**.

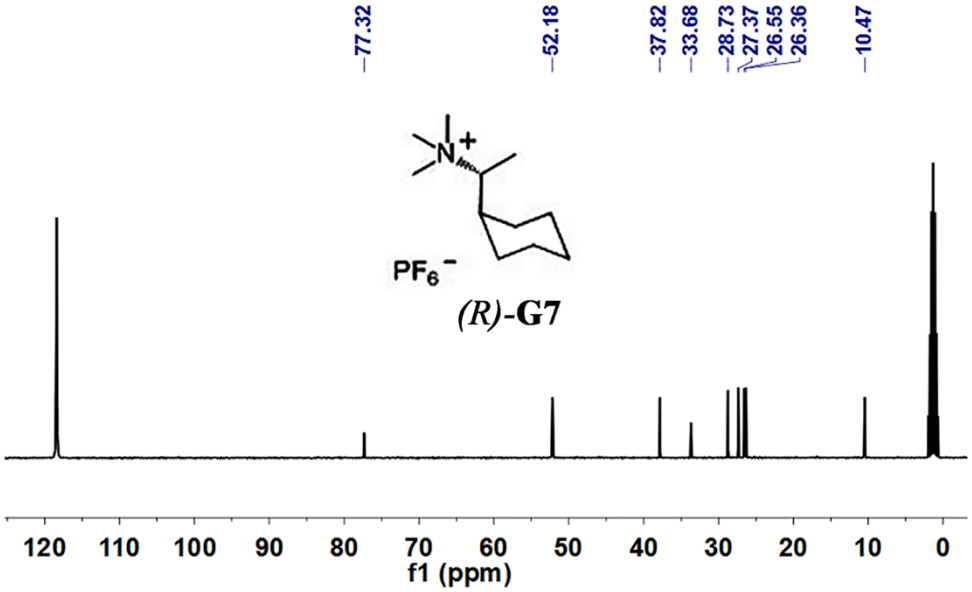

Fig. S18. ^{13}C NMR spectrum (100 MHz, MeCN-d_3) of *(R)*-**G7**.

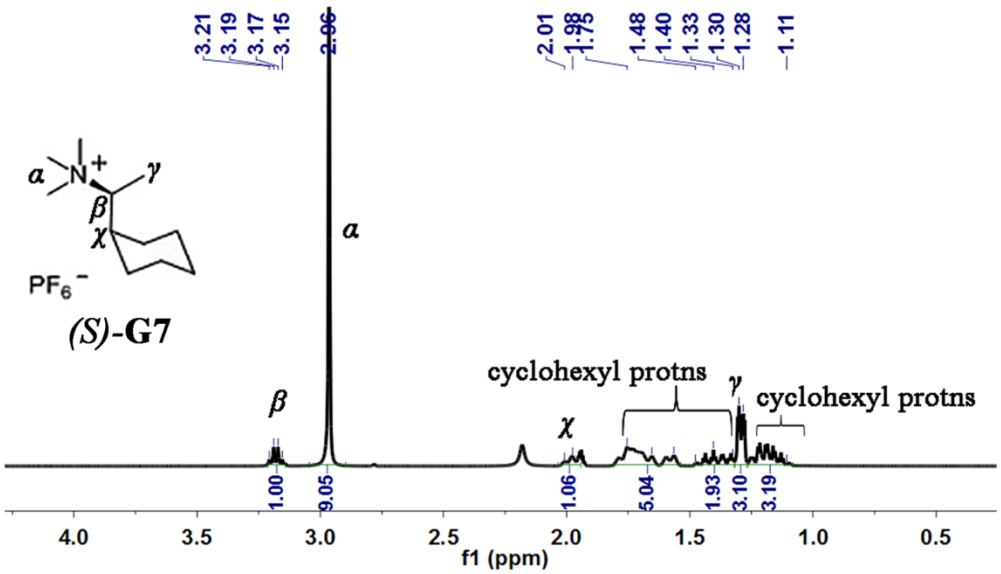

Fig. S19. ^{1}H NMR spectrum (400 MHz, MeCN-d_3) of *(S)*-**G7**.

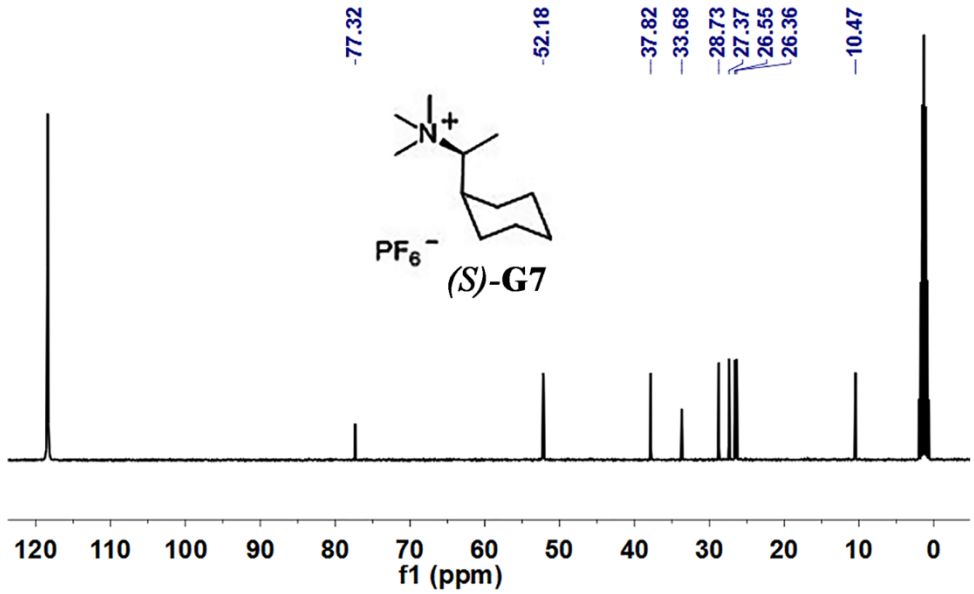

Fig. S20. ^{13}C NMR spectrum (100 MHz, MeCN-d_3) of *(S)*-**G7**.

3. NMR spectra of the host-guest complexes

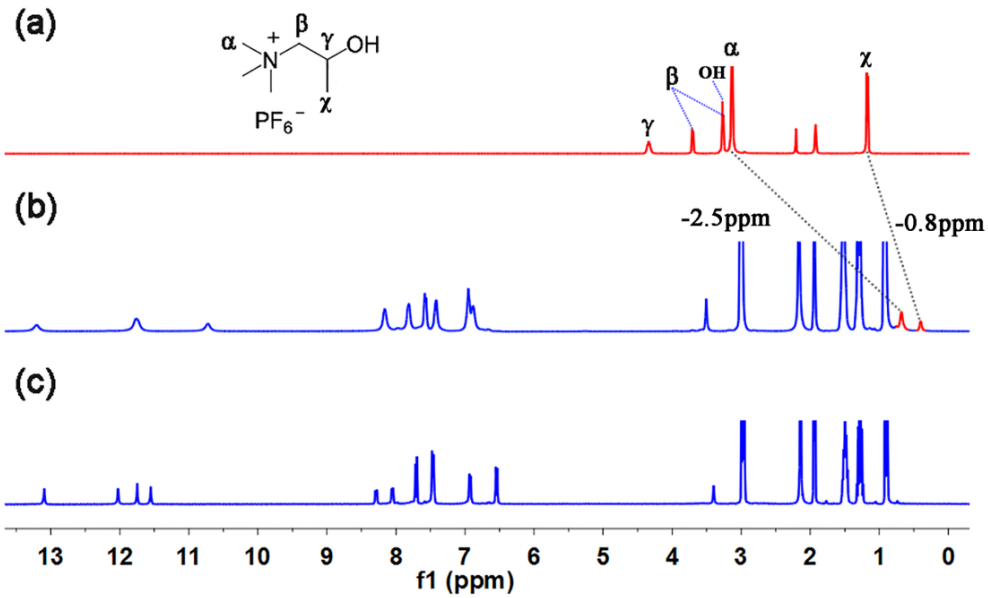

Fig. S21. ^{1}H NMR (400 MHz, MeCN-d_3) spectra of (a) ±**G2**, (b) **H** + 1.0 equiv. ±**G2** and (c) **H** (host).

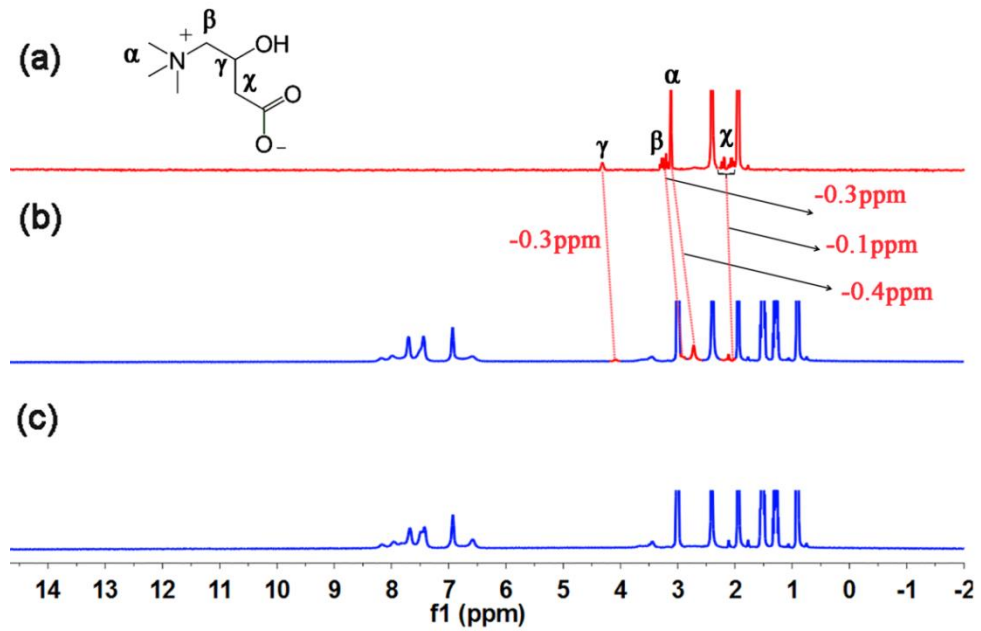

Fig. S22. ^{1}H NMR (400 MHz, MeCN-d_3/2% D_2O) spectra of (a) ±**G3**, (b) **H** + 1.0 equiv. ±**G3** and (c) **H**.

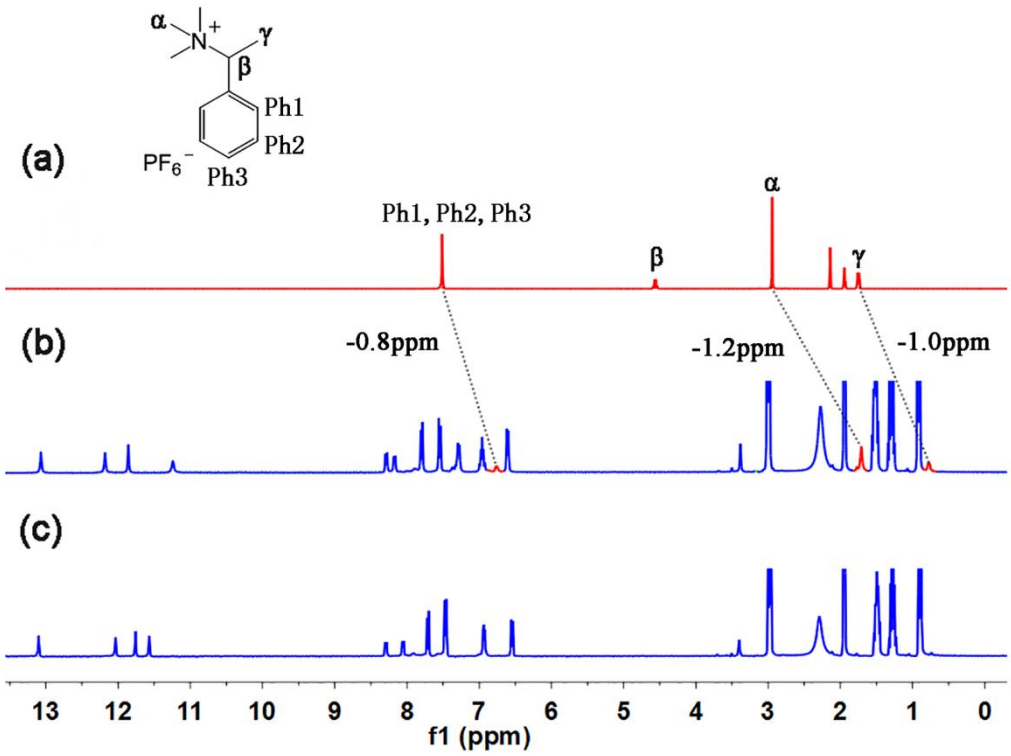

Fig. S23. ^{1}H NMR (400 MHz, MeCN-d_3) spectra of (a) ±**G4**, (b) **H** + 1.0 equiv. ±**G4** and (c) **H**.

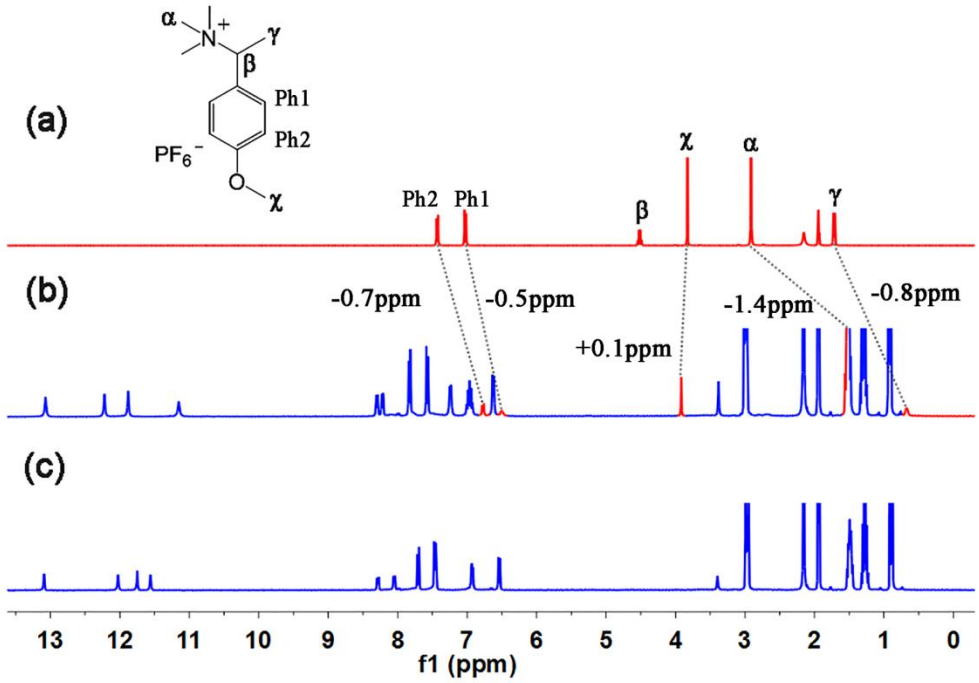

Fig. S24. ^{1}H NMR (400 MHz, MeCN-d_3) spectra of (a) ±**G5**, (b) **H** + 1.0 equiv. ±**G5** and (c) **H**.

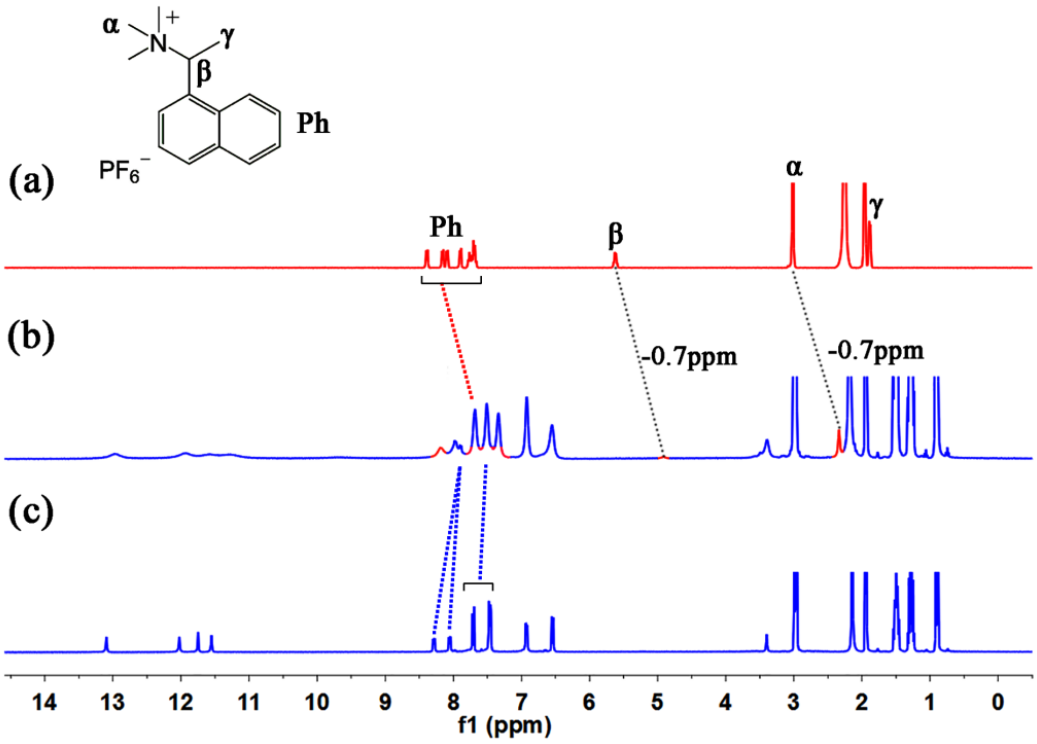

Fig. S25. ^{1}H NMR (400 MHz, MeCN-d_3) spectra of (a) ±**G6**, (b) **H** + 1.0 equiv. ±**G6** and (c) **H**.

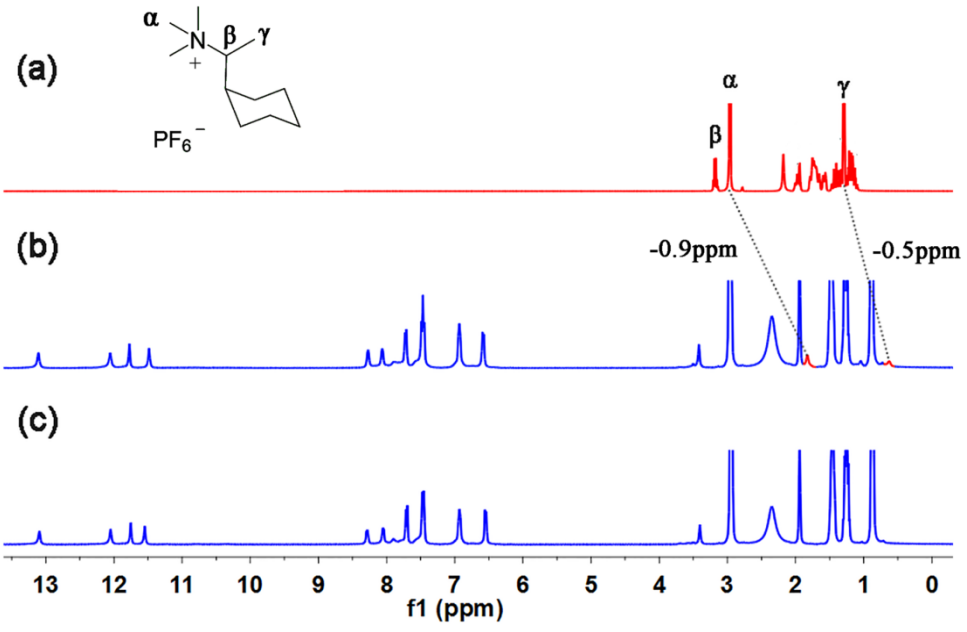

Fig. S26. ^{1}H NMR (400 MHz, MeCN-d_3) spectra of (a) ±**G7**, (b) **H** + 1.0 equiv. ±**G7** and (c) **H**.

4. Crystal structural data of $(TBA)_5[(\pm G1)\subset(PO_4)_2L_3]$

Table S1. Hydrogen bonds [Å and °] in the crystal structure of ±**G1**⊂**H**, $(TBA)_5[(\pm\mathbf{G1})\subset(PO_4)_2\mathbf{L}_3]$.

D–H···*A*	*d*(*D*–H)	*d*(H···*A*)	*d*(*D*···*A*)	∠(*D*H*A*)
N2–H2A···O25	0.88	1.89	2.754(2)	167
N3–H3A···O28	0.88	1.91	2.773(19)	165
N4–H4···O28	0.88	1.91	2.7689(19)	166
N5–H5A···O27	0.88	1.91	2.786(2)	177
N6–H6A···O29	0.88	1.94	2.7953(18)	163
N7–H7···O30	0.88	1.94	2.8109(19)	169
N8–H8···O30	0.88	2.06	2.884(2)	156
N9–H9A···O31	0.88	1.86	2.7331(19)	171
N12–H12'···O25	0.88	1.87	2.741(2)	172
N13–H13···O26	0.88	1.87	2.719(2)	160
N14–H14···O26	0.88	1.92	2.784(2)	167
N15–H15···O28	0.88	1.98	2.8389(19)	164
N17–H56'···O29	0.88	2.11	2.8710(19)	144
N18–H18···O29	0.88	1.93	2.7876(19)	163
N19–H50'···O31	0.88	1.96	2.766(2)	152
N22–H22···O27	0.88	2.10	2.904(2)	152
N23–H23A···O27	0.88	1.87	2.732(2)	164
N24–H24A···O27	0.88	2.12	2.992(2)	170
N25–H25···O26	0.88	1.92	2.764(2)	160
N26–H26A···O30	0.88	1.94	2.820(2)	177
N27–H27A···O32	0.88	2.37	3.066(2)	136
N28–H28···O32	0.88	1.88	2.7244(19)	160
N29–H29···O32	0.88	1.98	2.8076(19)	155
Average	0.88	1.97	2.8096	162

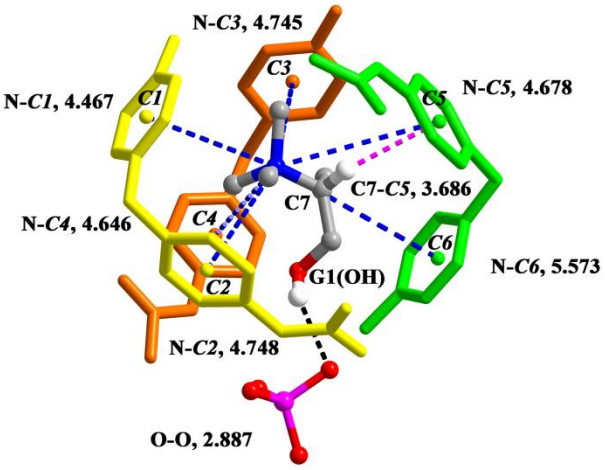

Fig. S27. Host-guest interactions in the crystal structure of ±**G1**⊂**H**, $(TBA)_5[(\mathbf{G1})\subset(PO_4)_2\mathbf{L}_3]$, wherein N•••centroid distances are shown as blue dashed lines for evaluating the cation-π interactions (in average, 4.810 Å) and the hydrogen bond between OH (**G**) and PO_4^{3-} (**H**) is shown as a black dashed line (O···O distance = 2.887 Å, ∠OHO = 170°), the CH···π interactions between C7-H (±**G1)** with one phenyl ring of **H** is shown as a purple dashed line.

5. NMR and HRMS studies of ±G1⊂H

5.1 Protons of L in H and ±G1⊂H were assigned according to COSY and NOESY spectra

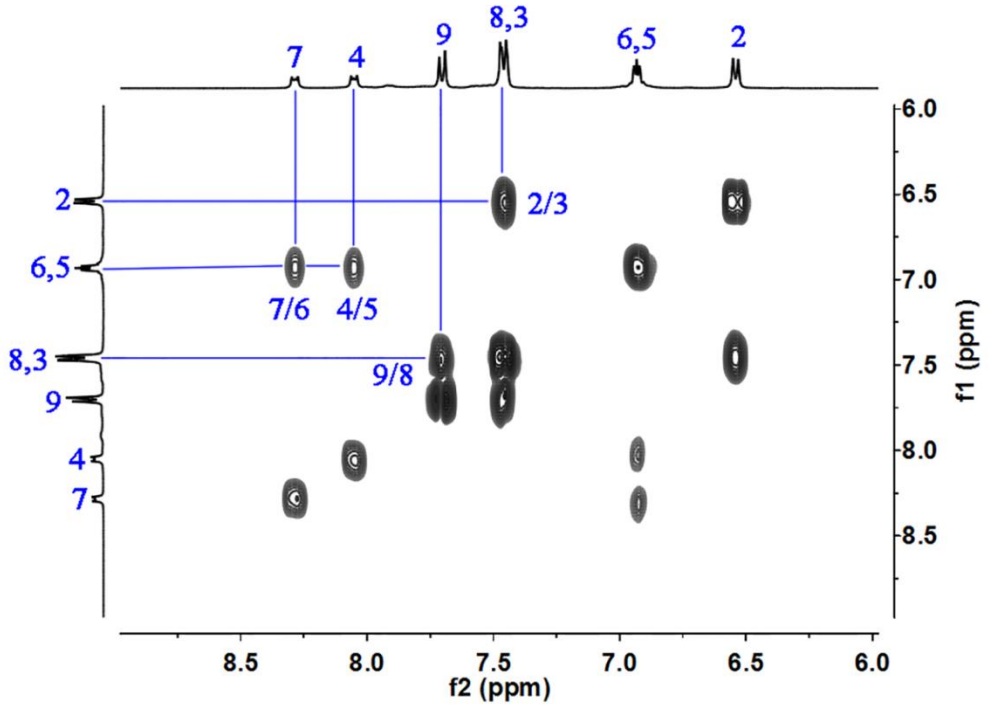

Fig. S28. Selected part of ^{1}H-^{1}H COSY spectra of **H** (400 MHz, MeCN-d_3).

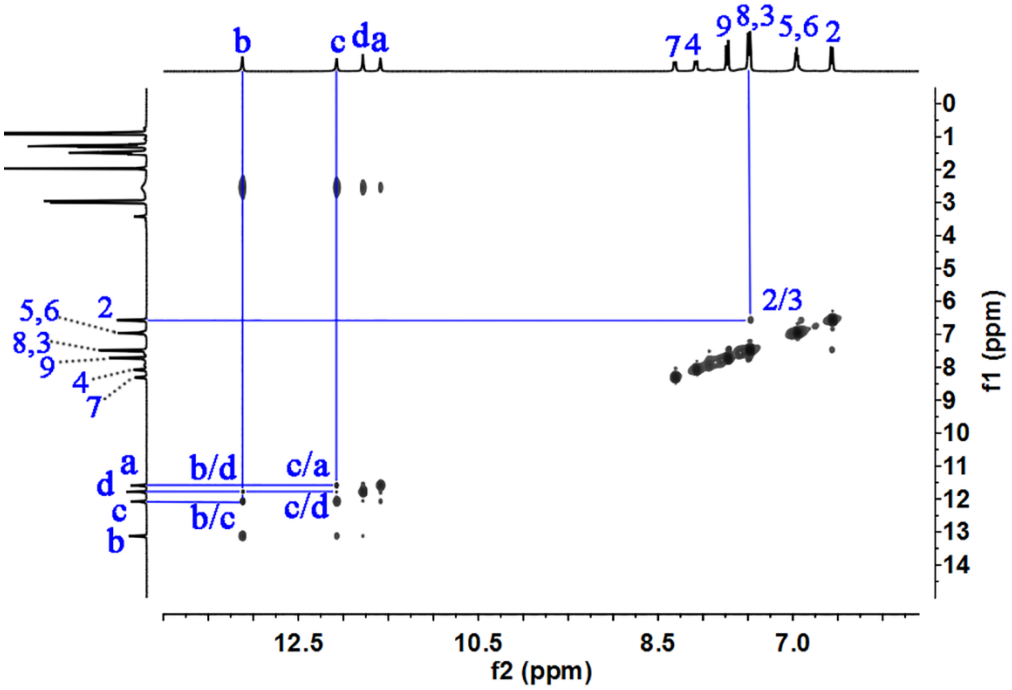

Fig. S29. Selected part of ^{1}H-^{1}H NOESY spectra of **H** (400 MHz, MeCN-d_3).

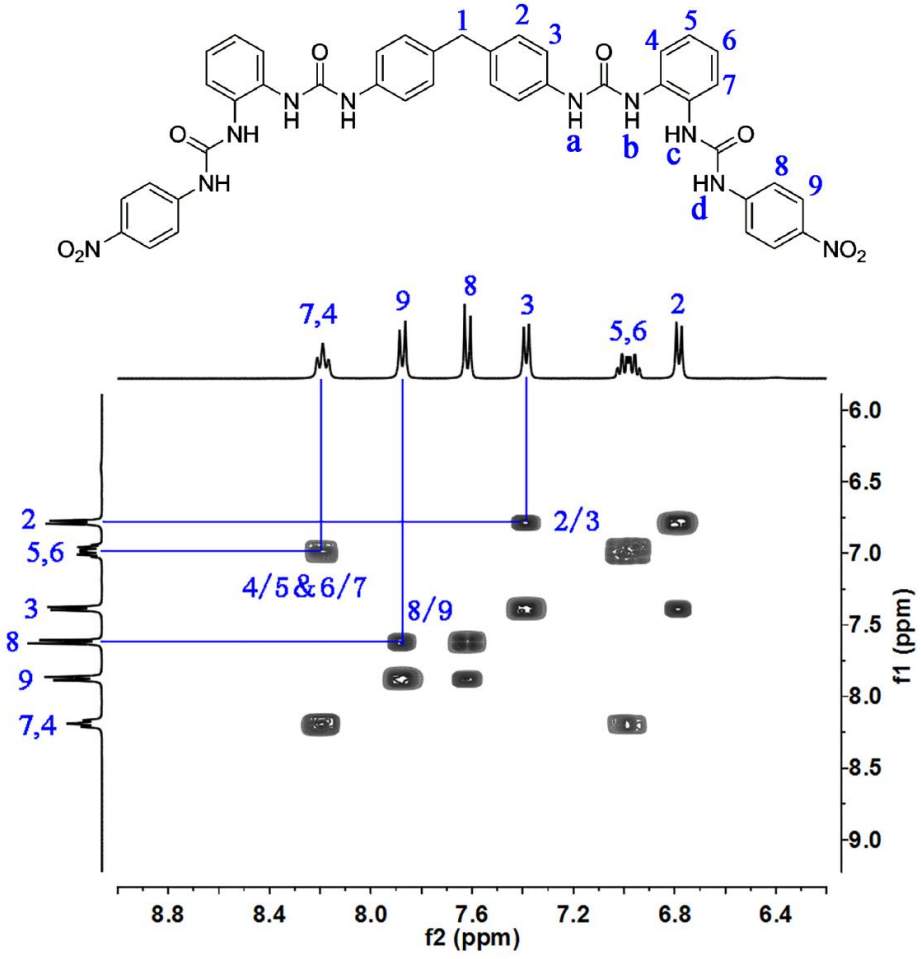

Fig. S30. Selected part of ^{1}H-^{1}H COSY spectra (400 MHz, MeCN-d_3) of ±**G1**⊂**H**.

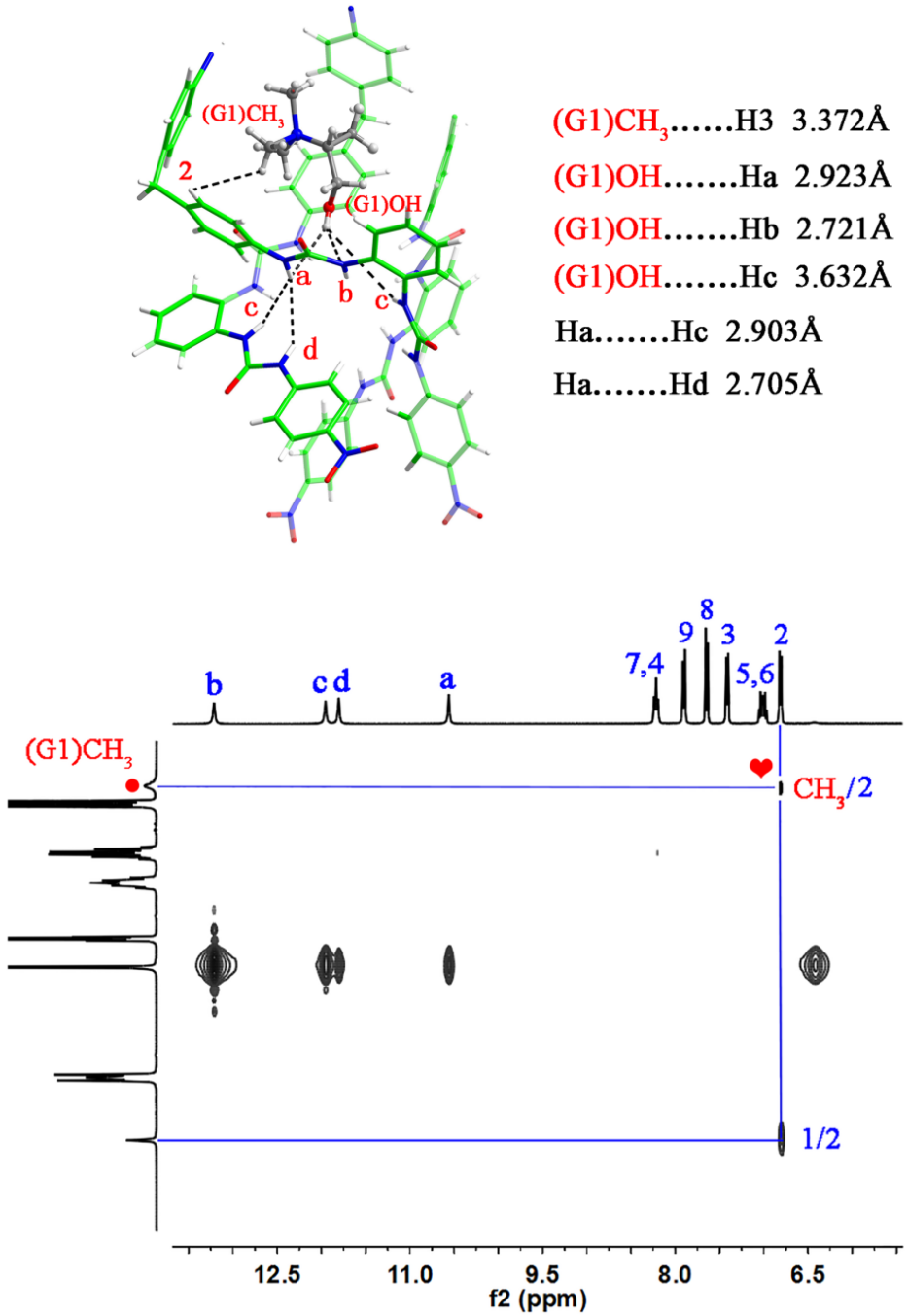

Fig. S31. Selected part of ^{1}H-^{1}H NOESY spectra (400MHz, MeCN-d_3) of ±**G1⊂H**.

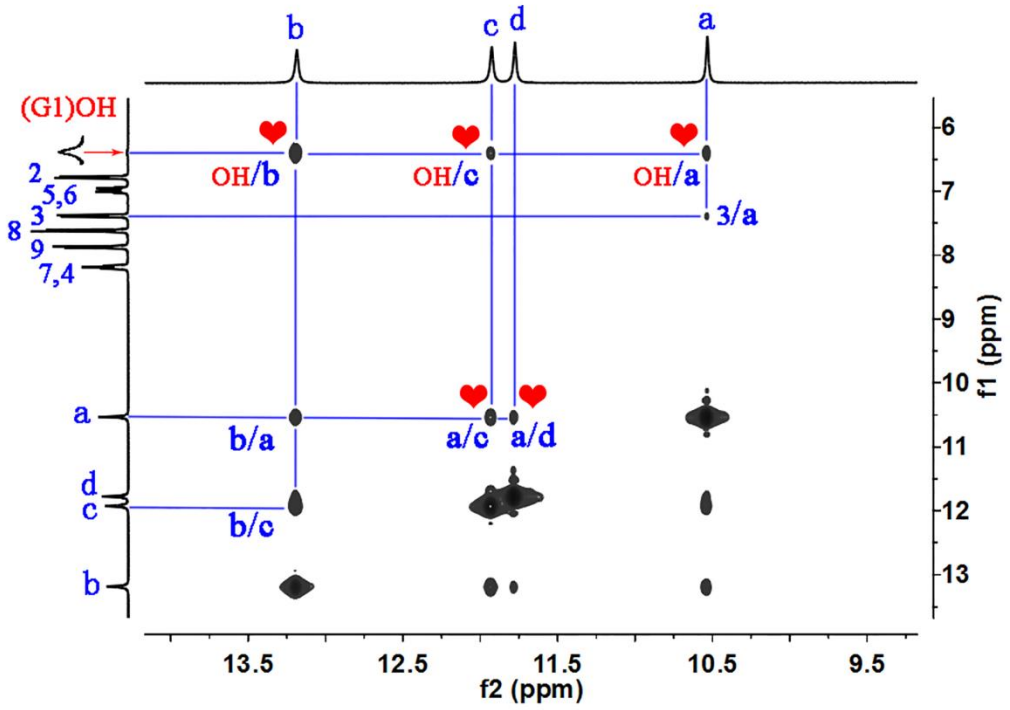

Fig. S32. Selected part of ^{1}H-^{1}H NOESY spectra (400 MHz, MeCN-d_3) of ±**G1**⊂**H**.

5.2 Protons of OH, Hα, Hγ of G1 in the spectrum of ±G1⊂H were assigned according to integral and reasonable chemical shifts

In the NMR spectra of ±**G1** ⊂**H** (Figure S33a), the peak at 6.4 ppm was attributed the OH signal of ±**G1** according to the integral and reasonable downfield shifts after formation of hydrogen bonds with the phosphate ion. The signal was so weak that the signal did not show clear signal in the COSY spectra. However, strong correlations between this signal (at 6.4 ppm) and adjacent protons (NHa, NHb and NHc) were observed in the NOESY spectrum of ±**G1**⊂**H** (Figure S32), which was consistent with the crystal structure. To exclude the possibility of impurity, 5 μL D_2O was added to the 0.5 mL MeCN-d_3 solution of ±**G1**⊂**H** (2 mM) to allow deuterium exchange with active protons. Consistently, the signal at 6.4 ppm disappeared after 10 minutes, indicating it was the signal of an active proton (Figure S33b). On the other hand, addition of 2.0 equiv. of $HClO_4$ induced disassembly of the ±**G1**⊂**H** complex, and the signal at 6.4 ppm disappeared at the same time, which was consistent with the release of ±**G1** (Figure S33c).

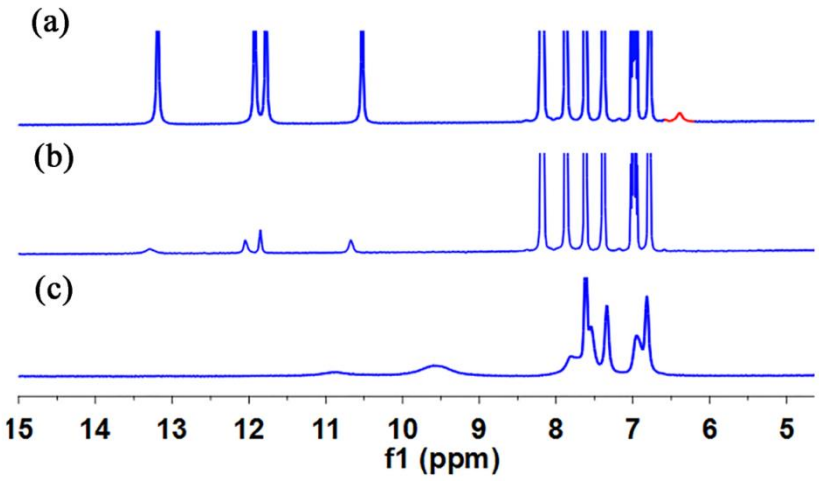

Fig. S33. ^{1}H NMR (400 MHz, MeCN-d_3) spectra of (a) ±**G1**⊂**H**, (b) ±**G1**⊂**H** + D_2O, and (c) ±**G 1**⊂**H** + $HClO_4$ ([±**G1**⊂**H**]) = 2.0 mM).

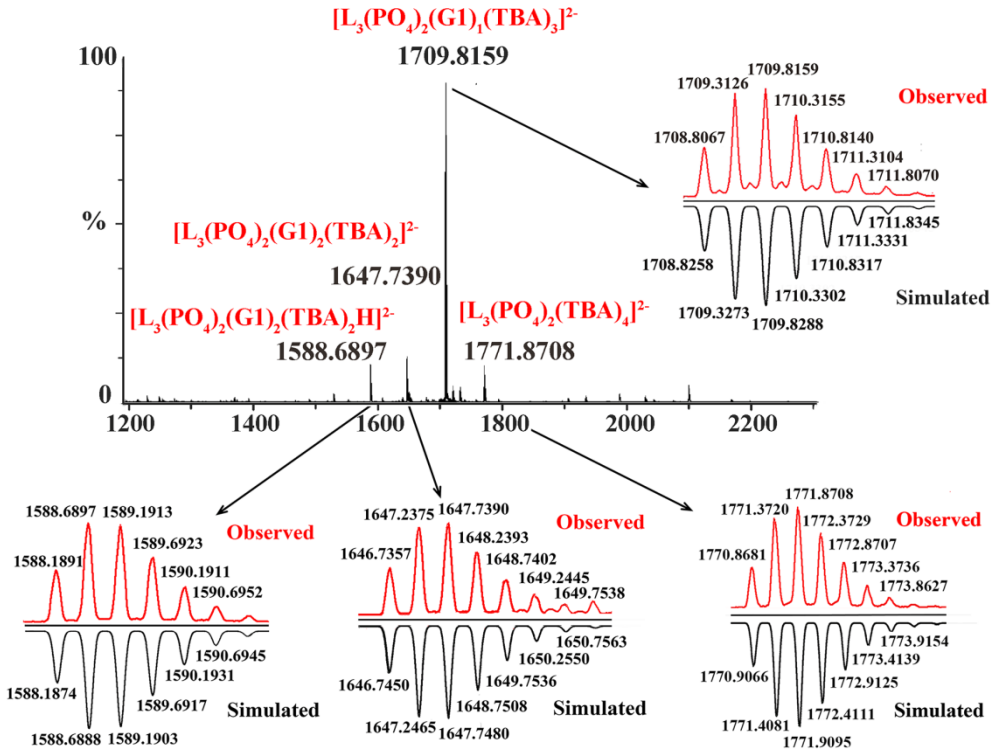

Fig. S34. HR-ESI-QTOF mass spectrum of ±**G1**⊂**H**, confirming the identity of the host-guest assembly.

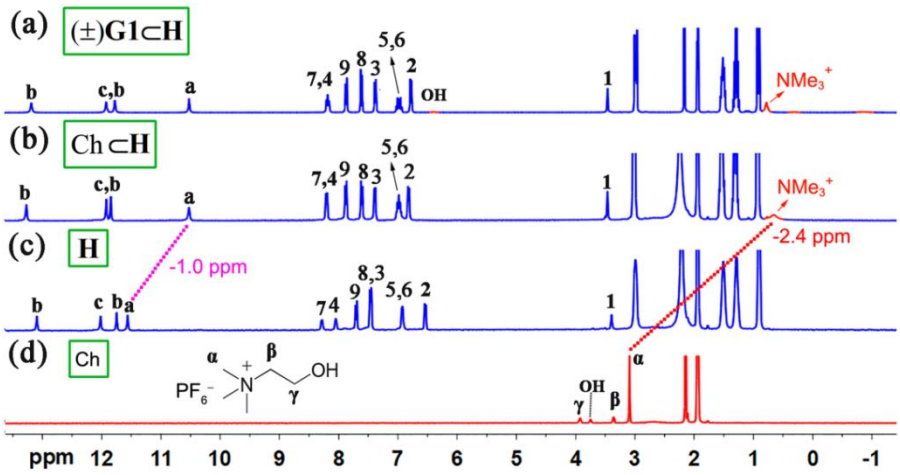

Fig. S35. ^{1}H NMR (400 MHz, MeCN-d_3) spectra of (a) **H** + 1.0 equiv. ±**G1**, (b) **H** + 1.0 equiv. Ch•PF_6, (c) **H** and (d) Ch•PF_6.

6. Density Functional Theory (DFT) computations

The geometry optimizations were performed with Turbomole V7.1 software.[2] The Density Functional Theory (DFT) method, augmented with empirical dispersion term (D3),[3] has been utilized. The B-LYP functional[4,5] and def2-SVP basis sets[6] were employed. COSMO implicit solvation model[7] was used to account for the solvation effect. SCF convergence criterion was set to 7 and the integration grid was m4, both in Turbomole's notation. Single point calculations employing def2-TZVPP basis sets were further performed to improve the energy.

The initial structures were either imported from crystal data directly or modified manually from similar experimental structures.[8] The host cages were always taken from crystal structures. Semiempirical PM6 optimizations[9] were performed for geometry relaxations before DFT calculations. The vibrational contributions to free energies were obtained at gas-phase PM6 level. Due to the high similarities between the two configurations of each host-guest complex, the thermodynamic corrections were close as expected.

In addition, another functional, i.e. M06-2X [10] was employed to verify the results from BLYP-D3, starting from the BLYP-D3 converged structures by using the Gaussian09 [11] package. Nearly converged results were obtained, and the changes of the total energies are below 10^{-4} a.u. bar. However, we encountered a situation of small energy oscillation which could not be solved after many attempts, possibly due to the flexible nature of our molecules. Nevertheless, the lower energies from the current optimization were picked, and the ΔG for the two models of Ch⊂(*M*)-**H** (9.5 kcal/mol) is very close to that (9.7 kcal/mol) from BLYP-D3 (Table S2). Both geometries do not undergo major changes during the whole optimization processes. Thus, the preliminary results suggest that the two methods agree with each other in this case.

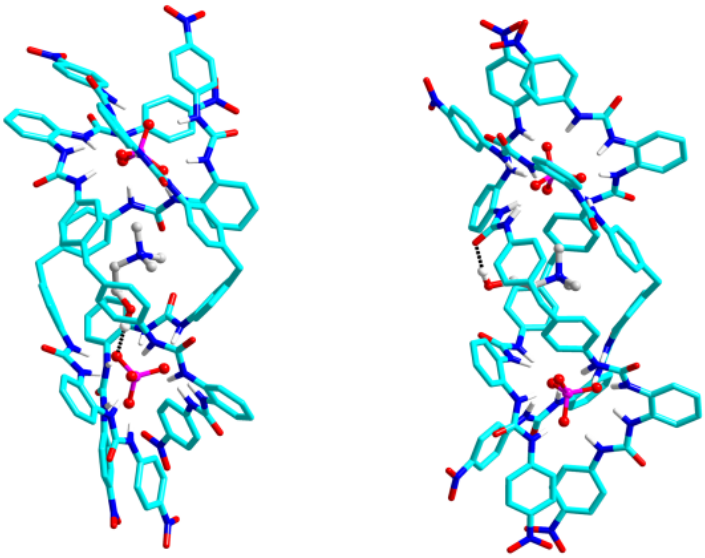

Fig. S36. DFT optimized structures of Ch⊂(*M*)-**H** in binding mode I (left) and II (right).

Table S2. DFT calculated energies of Ch⊂(*M*)-**H** in two binding mode.

	E/a.u.	Rel. E (kcal.mol^{-1})	Δ/a.u.	Rel. G (kcal.mol^{-1})
mode I	-9801.984083486	0	1.937199	0
mode II	-9801.966136266	11.26	1.934744	9.72

Note: mode II is the molecule structure published on *Nature Communications*.[8]
Free energy G = E + Δ; Δ is the thermal correction to Gibbs free energy, at the PM6 level, gas phase.

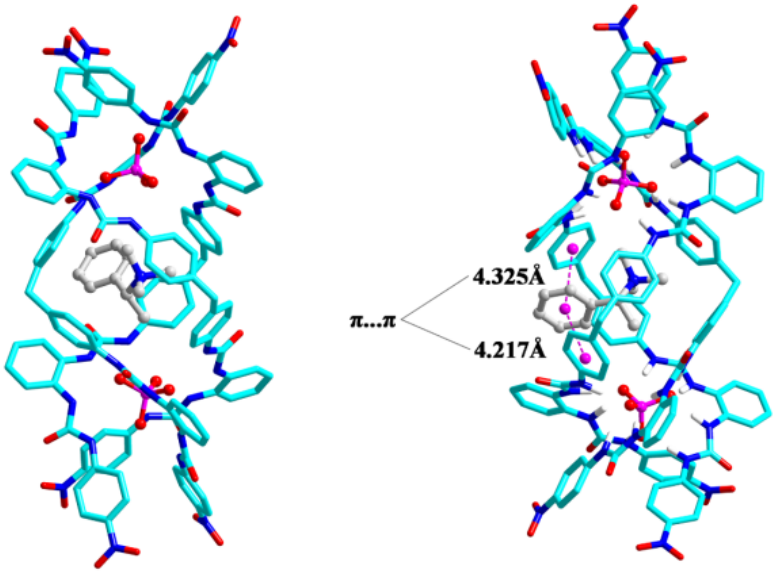

Fig. S37. DFT optimized structures of *(R)*-**G4**⊂(*M*)-**H** (left) and *(R)*-**G4**⊂(P)-**H** (right).

Table S3. DFT calculated energies of *(R)*-**G4**⊂(*M*)-**H** and *(R)*-**G4**⊂(*P*)-**H**.

	E/a.u.	Rel. E (kcal.mol^{-1})	Δ/a.u.	Rel. G (kcal.mol^{-1})
P-GR	-9957.609557545	0	2.003120	0
M-GR	-9957.593018409	10.4	2.003632	10.7

Note: free energy G = E + Δ; Δ is the thermal correction.

7. CD spectra of guests and host-guest complexes

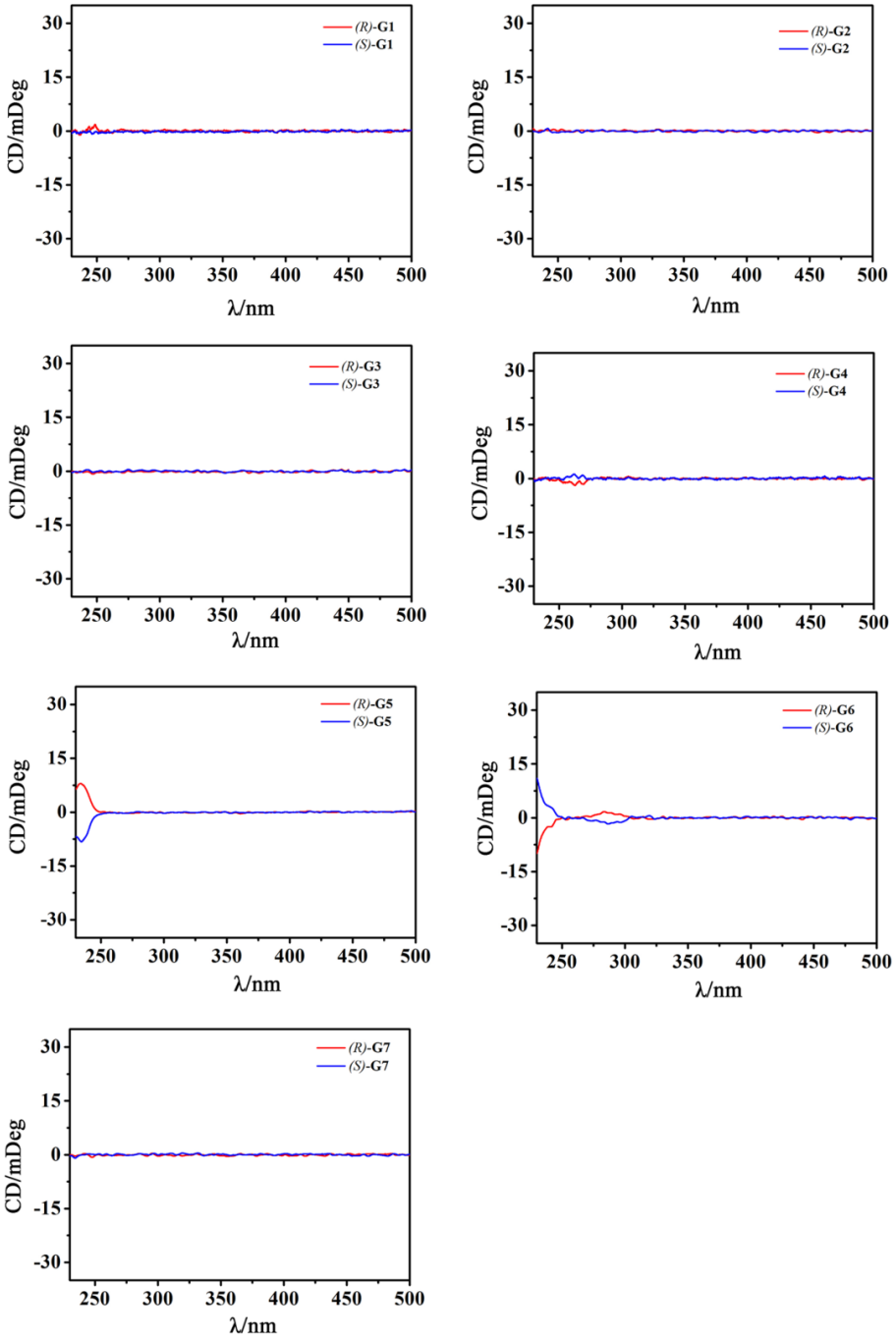

Fig. S38. CD spectra of enantiomers of **G1**-**G7** (100 μM, MeCN).

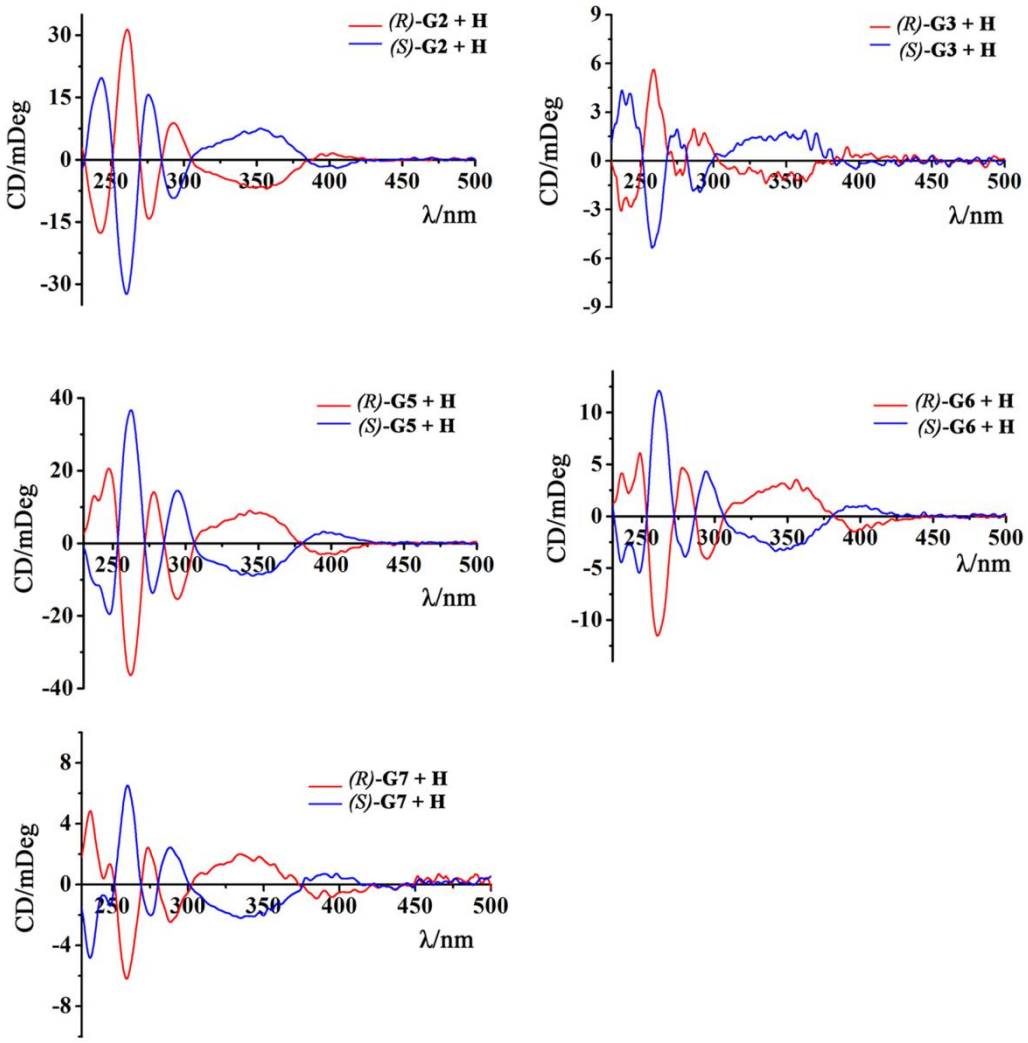

Fig. S39. CD spectra of **H** (10 μM, MeCN) in the presence of 1.0 equiv of enantiomers of **G2**, **G3**, and **G5**-**G7**.

8. CD Titrations

8.1 Determination of binding constants by CD titrations

All CD titrations were performed at room temperature. In the titrations of **G** with **H**, successive addition of known amounts of **G** was added to a 3 mL solution of **H** (10 μM) in MeCN. To keep the concentration of **H** constant in the titration course, stock solutions of analytes ([±**G1**] = [±**G2**] = 1.0 mM, [±**G4**] = [±**G5**] = 5.0 mM, [±**G6**] = 2.5 mM, [±**G7**] = 10 mM,) were prepared with a 10 μM solution of **H** in MeCN. One except is that 0.05 M, 0.1M, 0.5 M and 1.0 M stock solutions of ±**G3** were prepared in H_2O due to the low solubility of ±**G3** in MeCN, which totally introduced 0.6% (v/v%) H_2O in the titration course and the influence of this tiny amount of water was ignored.

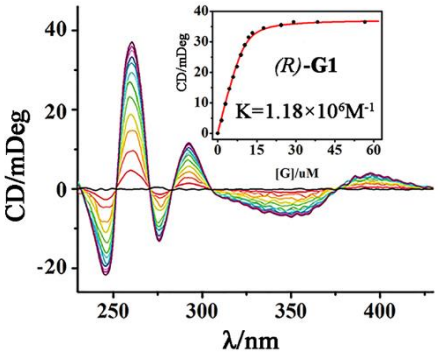
CD/mDeg
λ/nm
(R)-G1
K=1.18×10⁶M⁻¹
[G]/uM

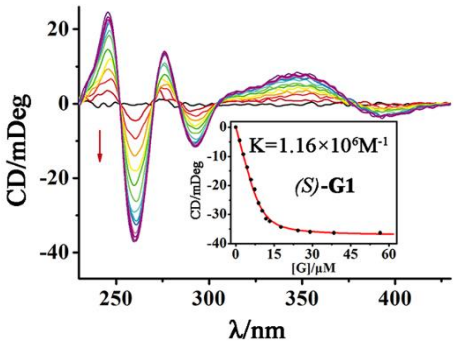
CD/mDeg
λ/nm
K=1.16×10⁶M⁻¹
(S)-G1
[G]/μM

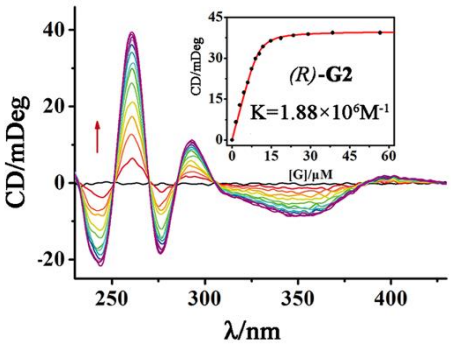
CD/mDeg
λ/nm
(R)-G2
K=1.88×10⁶M⁻¹
[G]/μM

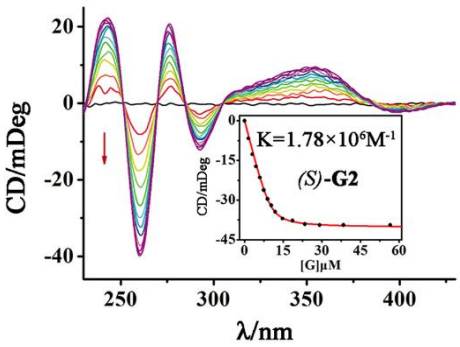
CD/mDeg
λ/nm
K=1.78×10⁶M⁻¹
(S)-G2
[G]μM

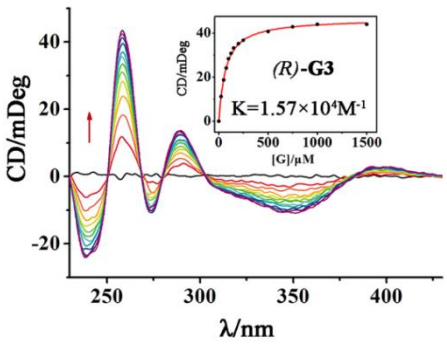
CD/mDeg
λ/nm
(R)-G3
K=1.57×10⁴M⁻¹
[G]/μM

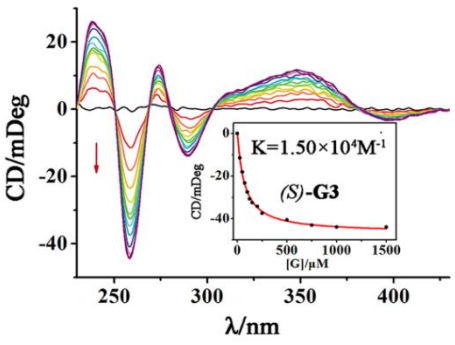
CD/mDeg
λ/nm
K=1.50×10⁴M⁻¹
(S)-G3
[G]/μM

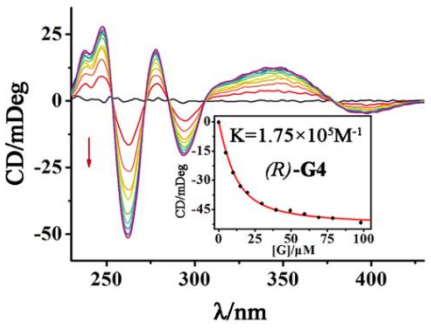
CD/mDeg
λ/nm
K=1.75×10⁵M⁻¹
(R)-G4
[G]/μM

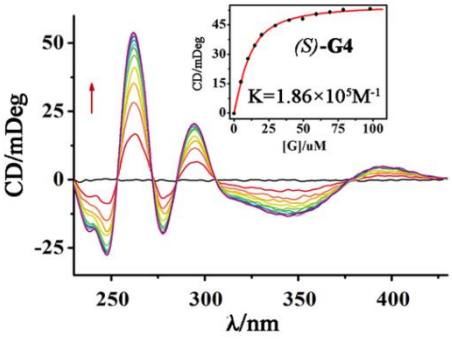
CD/mDeg
λ/nm
(S)-G4
K=1.86×10⁵M⁻¹
[G]/uM

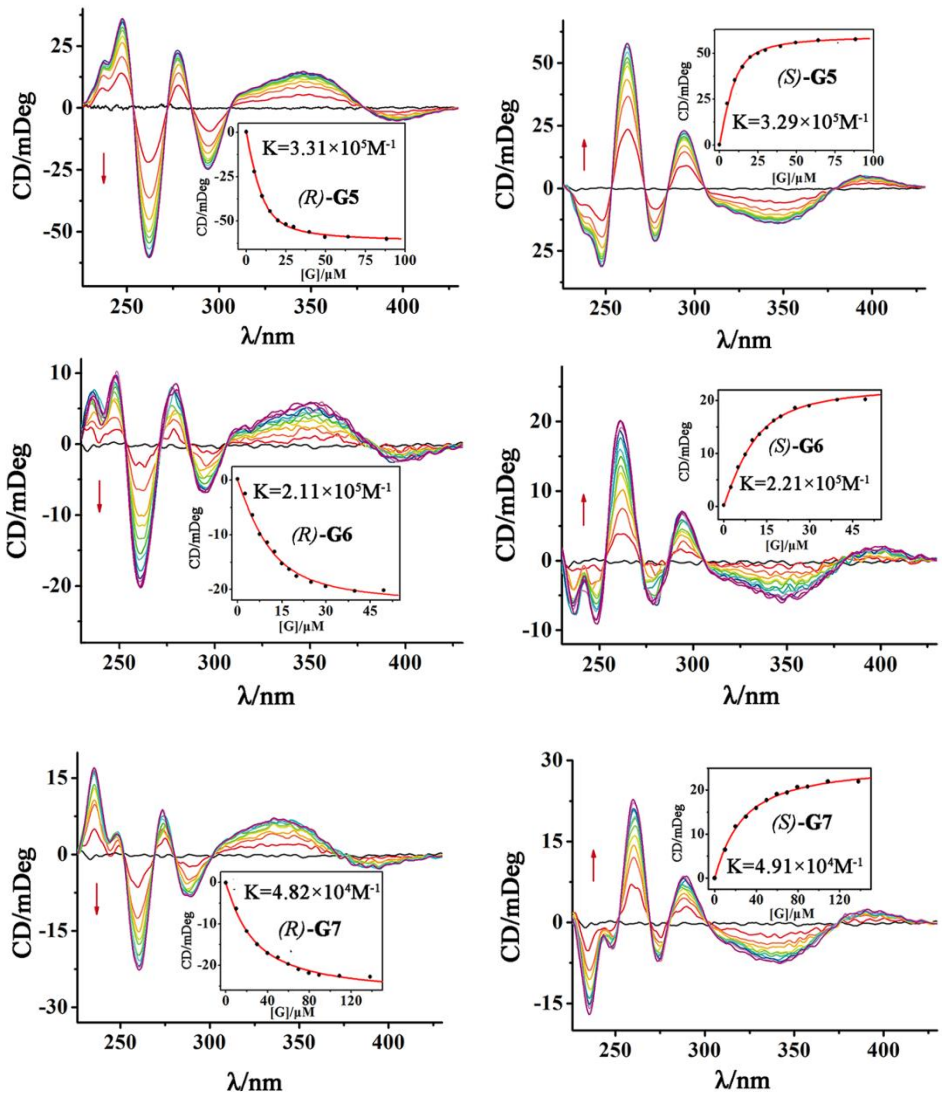

Fig. S40. CD spectra of **H** as a function of the concentration of enantiomers of **±G1**-**±G7**. Insets: association constants determined by fitting the titration curves at λ = 261 nm (**±G1**, **±G2,** **±G6**), 259 nm (**±G3**, **±G7**), 262 nm (**±G4**, **±G5**) to a 1:1 (host : guest) binding mode by the Dynafit program (errors < 10%).

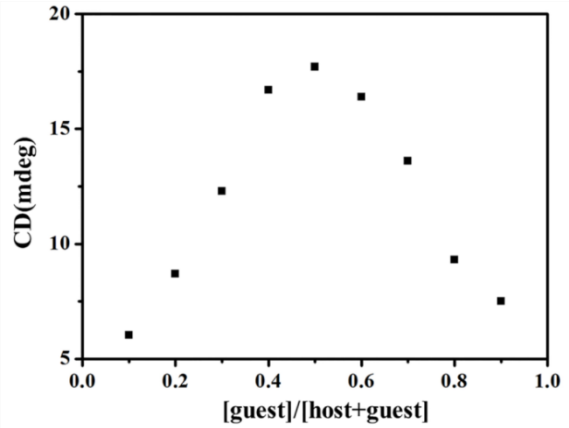

Fig. S41. Job's plot analysis of **H** (host) with *(R)*-**G1** (guest) in MeCN. ([**H**] + [*(R)*-**G1**] = 10 μM). The CD intensities at λ = 261 nm were plotted against the molar fraction of the guest.

A Typical Script File of (*R*)-**G1** for Dynafit Input:
Guest (G) is varied while a CD active Host (H*) is held constant.Fit CD increase to 1:1 binding model. Method refer to J. Biol. Chem. 267, 22054 (1992).

```
;_____________________________________________________________
[task]
    data = equilibrium
    task = fit
[mechanism]
    H*G <==> H* + G     :       Ka      assoc
[constants]
    Ka = 1.18?
[concentrations]
    H* = 10    ; Corresponding to [H] = 10 vM-1
[responses]
    H*    = 0      ; CD/[H] of H* without Guest
    H*G =3.7623    ; Ideal CD/[H*G] of H*G
[data]
    variable         G
    set              H
[output]
directory ./CDoutput/(R)-G1
[set:H]
G,vM                 CD/mDeg
0                      0
1.49775337         4.2159
2.991026919        9.6242
4.479840717        14.6022
5.964214712        18.4770
7.444168734        21.8878
8.919722498      25.6834
10.3908956       28.9233
11.85770751      31.4650
13.3201776       32.8960
17.68172888      34.5070
24.3902439       35.5070
29.12621359      36.5075
38.46153846      36.5070
56.60377358      36.5070
[end]
```

8.2 Data for chiroptical sensing.

Method of ee determination:

All CD titrations were performed at room temperature. Stock solutions of analytes **±G1**-**±G7** (10 mM) were prepared in MeCN. For the ee calibration titrations and "unknown" sample detection, saturated concentrations of **±G1**-**±G7** with varied ee values (ee based on (*R*)-**G**, +100, +80, +60, +40, +20, 0, -20, -40, -60, -80, -100 ee for calibration samples and five randomly selected values for "unknown" samples) were added to a 3 mL solution of **H** (10 μM) in MeCN. One except is that 84 mM stock solution of **±G3** was prepared in H_2O due to the low solubility of **±G3** in MeCN, which totally introduced 0.6% (v/v%) H_2O in the titration course and the influence of this tiny amount of water was ignored.

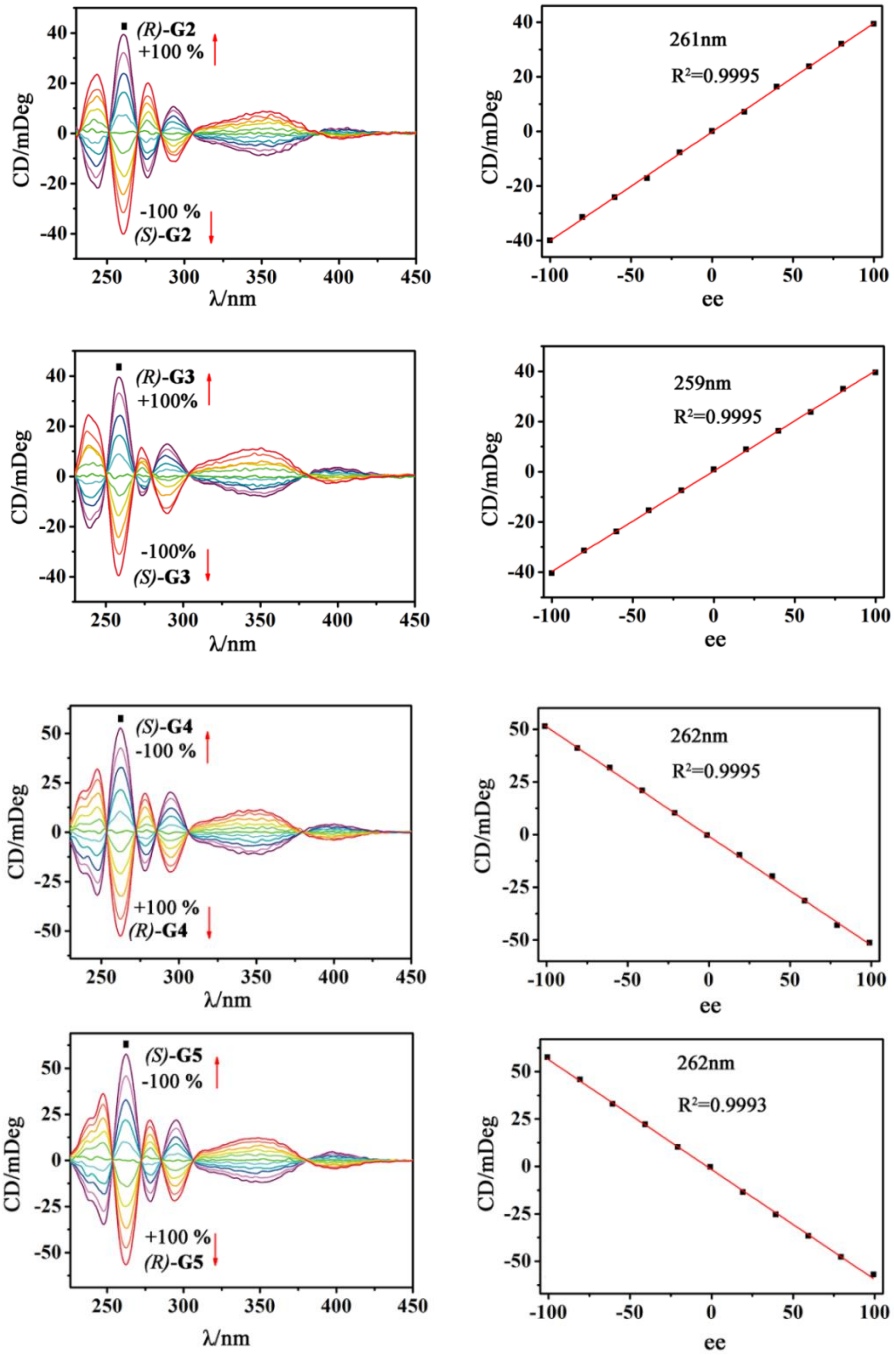

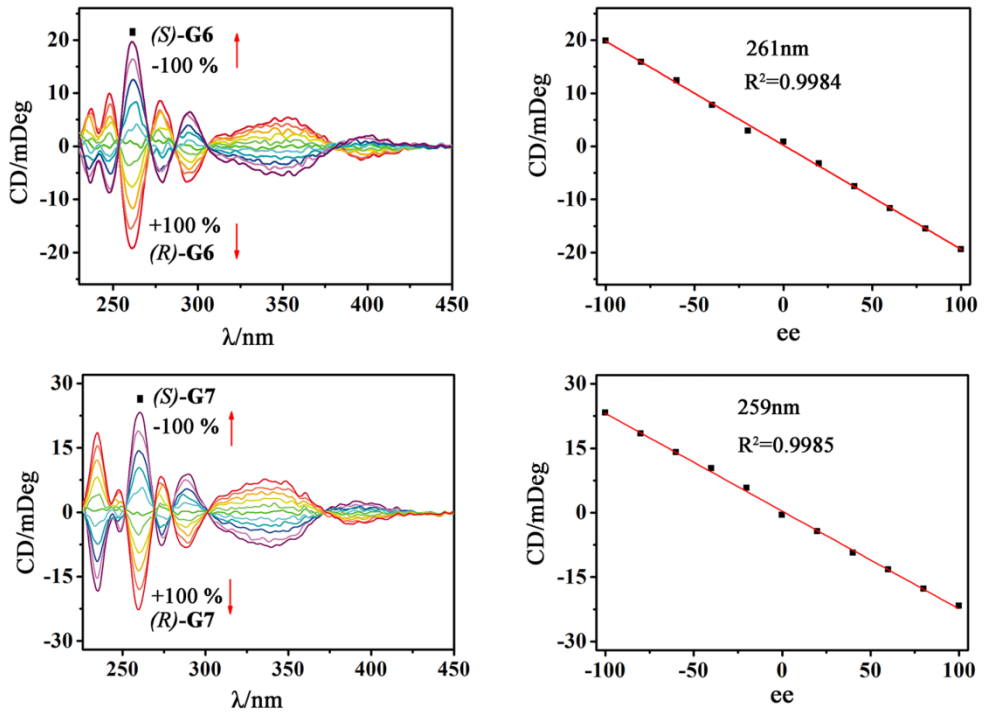

Fig. S42. CD spectra of **H** (10 μM) in the presence of saturated solution of guests ([**G1**] = [**G2**] = 20 μM, [**G3**] = 500 μM, [**G4**] = [**G5**] = 60 μM, [**G6**] = 40 μM, [**G7**] = 80 μM, with various ee values (left) and the corresponding ee calibration plots (right) for the CD signal at the respective wavelength (259-262 nm).

Table S4. Calculated ee from calibration lines and the absolute errors.

	Actual ee (%)	Experimental ee (%)	Absolute Error (%)
G1	70.0	70.6	0.6
	30.0	30.8	0.8
	-10.0	-9.3	0.7
	-50.0	-48.4	1.6
	-90.0	-88.6	1.4
			In average ±1.0
G2	70.0	70.9	0.9
	50.0	51.8	1.8
	30.0	29.4	0.6
	-10.0	-10.5	0.5
	-90.0	-91.6	1.6
			In average ±1.1
G3	70.0	72.0	2.0
	30.0	27.6	2.4
	-10.0	-9.7	0.3
	-50.0	-48.1	1.9
	-90.0	-89.0	1.0
			In average ±1.5
G4	90.0	90.5	0.5
	50.0	52.7	2.7
	30.0	28.4	1.6
	-10.0	-9.6	0.4
	-70.0	-68.7	1.3

			In average ±1.3
G5	90.0	88.2	1.8
	10.0	7.8	2.2
	-30.0	-29.1	0.9
	-50.0	-49.2	0.8
	-70.0	-71.2	1.2
			In average ±1.4
G6	90.0	88.3	1.7
	70.0	68.2	1.8
	30.0	28.3	1.7
	-10.0	-9.0	1.0
	-50.0	-52.7	2.7
			In average ±1.8
G7	90.0	87.0	3.0
	50.0	51.7	1.7
	10.0	-9.8	0.2
	-30.0	-31.6	1.6
	-70.0	-71.0	1.0
			In average ±1.5

References

1. G.-W. Zhang, P.-F. Li, Z. Meng, H.-X. Wang, Y. Han, C.-F. Chen, *Angew. Chem. Int. Ed.* 2016, **55**, 5304-5308.
2. TURBOMOLE V7.1 2016, a development of University of Karlsruhe and Forschungszentrum Karlsruhe GmbH, 1989-2007, TURBOMOLE GmbH, since 2007; available from http://www.turbomole.com.
3. S. Grimme, J. Antony, S. Ehrlich and H. Krieg, *J. Chem. Phys.* 2010, **32**, 154104.
4. A. D. Becke, *Phys. Rev. A*, 1988, **38**, 3098-3100.
5. C. Lee, W. Yang and R. G. Parr, *Phys. Rev. B*, 1988, **37**, 785-789.
6. F. Weigend and R. Ahlrichs, *Phys. Chem. Chem. Phys*. 2005, **7**, 3297-3305.
7. A. Klamt and G. Schüürmann, *J. Chem. Soc., Perkin Trans.* 1993, **2**, 799-805.
8. C. Jia, W. Zuo, D. Yang, Y. M. Chen, L. P. Cao, R. Custelcean, J. Hostaš, P. Hobza, R. Glaser, Y.-Yu. Wang, X.-J. Yang and B. Wu, *Nat. Commun*., 2017, **8**, 938.
9. James J. P. Stewart, *J. Mol. Model.*, 2007, **13**, 1173-1213.
10. Y. Zhao and D. Truhlar, *Theor. Chem. Acc.*, 2008, **120**, 215-241.
11. M. J. Frisch, G. W. Trucks, H. B. Schlegel, G. E. Scuseria, M. A. Robb, J. R. Cheeseman, G. Scalmani, V. Barone, B. Mennucci, G. A. Petersson, H. Nakatsuji, M. Caricato, X. Li, H. P. Hratchian, A. F. Izmaylov, J. Bloino, G. Zheng, J. L. Sonnenberg, M. Hada, M. Ehara, K. Toyota, R. Fukuda, J. Hasegawa, M. Ishida, T. Nakajima, Y. Honda, O. Kitao, H. Nakai, T. Vreven, J. A. Montgomery Jr., J. E. Peralta, F. Ogliaro, M. Bearpark, J. J. Heyd, E. Brothers, K. N. Kudin, V. N. Staroverov, T. Keith, R. Kobayashi, J. Normand, K. Raghavachari, A. Rendell, J. C. Burant, S. S. Iyengar, J. Tomasi, M. Cossi, N. Rega, J. M. Millam, M. Klene, J. E. Knox, J. B. Cross, V. Bakken, C. Adamo, J. Jaramillo, R. Gomperts, R. E. Stratmann, O. Yazyev, A. J. Austin, R. Cammi, C. Pomelli, J. W. Ochterski, R. L. Martin, K. Morokuma, V. G. Zakrzewski, G. A. Voth, P. Salvador, J. J. Dannenberg, S. Dapprich, A. D. Daniels, O. Farkas, J. B. Foresman, J. V. Ortiz, J. Cioslowski, and D. J. Fox. Gaussian 09, revision e.01. Gaussian, Inc., Wallingford CT, 2013.